Supporting Information

Organometallic Iridium Catalysts Based on Pyridine Carboxylate Ligands for the Oxidative Splitting of Water

Alberto Bucci,[a] *Arianna Savini,*[a] *Luca Rocchigiani,*[a] *Cristiano Zuccaccia,*[a] *Silvia Rizzato,*[b] *Alberto Albinati,*[b] *Antoni Llobet,*[c] *and Alceo Macchioni*[a*]

[a]Dipartimento di Chimica, University of Perugia, Via Elce di Sotto 8, Perugia, Italy

[b]Dipartimento di Chimica, University of Milano, Via Golgi 19, Milano, Italy

[c]Institute of Chemical Research of Catalonia, Avinguda Països Catalans 16, Tarragona, Spain

E-mail: alceo@unipg.it

Synthesis and characterization

Material and Methods. All reagents used for the syntheses in the present work were purchased from Sigma-Aldrich and used without additional purification. Reagent grade organic solvents were obtained from Sigma-Aldrich and dried by standard methods. Distilled water was further purified using a Milli-Q Ultrapure water purification system. $[Cp^*IrCl(\mu\text{-}Cl)]_2$ was prepared according to literature procedure.[1] Stock solutions of Ce^{+4} for kinetic measurements were prepared from $(NH_4)_2Ce(NO_3)_6$ (≥98.0%, Sigma-Aldrich). Acid solutions were prepared from concentrated HNO_3 (Trace Metal Grade, ≥65%, Sigma-Aldrich) and distilled, deionized water. NMR spectra were recorded at room temperature on a Bruker Avance DRX 400 spectrometer and referenced to the residual solvent peak (δ in ppm and *J* in Hz).

$[Cp^*Ir(\kappa^2\text{-}N,O)Cl]$ (κ^2-N,O = 2-pyridinecarboxylic acid, ion(-1)) (**1a**). This compound was synthesized in 70% overall yield slightly modifying the procedures reported in the literature.[2] $[Cp^*IrCl(\mu\text{-}Cl)]_2$ (100 mg, 0.126 mmol) and 3.0 equivalents of 2-pyridinecarboxylic acid (46.5 mg, 0.378 mmol) were dissolved in 30 mL of methanol at room temperature. A solution of 18 mg of KOH in MeOH was added to the mixture. The formation of a precipitate was immediately observed and the solution changed color from orange to yellow. After stirring for 1 h, the solution was concentrated under reduced pressure and left at -20°C overnight. The resulting solid was filtered off, washed with diethyl ether and dried under reduced pressure. ^1H NMR (400.13 MHz, DMSO-d_6): δ = 8.77 (d, 1H, J = 6.0 Hz), 8.12 (t, 1H, J = 5.0 Hz), 7.90 (d, 1H, J = 8.0 Hz), 7.75 (t, 1H, J = 7.0 Hz), 1.63 (s, 15H) ppm. $^{13}C\{^1H\}$ NMR (125.77 MHz, DMSO-d_6): δ = 171.7, 150.5, 150.3, 139.6, 129.1, 126.2, 84.9, 8.3 ppm.

[Cp*Ir(κ²-N,O)NO₃] (κ²-N,O = 2-pyridinecarboxylic acid, ion(-1)) (**1b**). 100 mg of **1a** (0.206 mmol) were dissolved in dichloromethane and 3 equivalents of $AgNO_3$ (105 mg, 0.618 mmol) were added. After stirring at room temperature for 18h, the formed precipitate was filtered out and washed with dichloromethane. The latter was removed from the filtered solution by evaporation and the solid obtained was dried under reduced pressure. ^{1}H and ^{13}C data were the same than those of **1a**. Anal. Calcd. for $C_{16}H_{19}IrN_2O_5$: C, 37.55; H, 3.74; N, 5.48. Found: C, 37.61; H, 3.75; N, 5.47.

[Cp*Ir(κ²-N,O)Cl] (κ²-N,O = 2,4-pyridinedicarboxylic acid, ion(-1),) (**2**). $[Cp^*IrCl(\mu\text{-}Cl)]_2$ (150 mg, 0.188 mmol) and 2.0 equivalents of 2,4-pyridinedicarboxylic acid (63 mg, 0.376 mmol) were dissolved in 15 mL of methanol at room temperature. A solution of 22 mg of KOH in MeOH was added to the mixture, which changed color from orange to yellow. After stirring for 1 h, the solution was concentrated under reduced pressure to 10 mL. 2 mL of diethyl ether were added and the mixture was left at -20°C for 3h. Finally the solid was filtered off, washed with diethyl ether and dried under reduced pressure (159 mg, 80%). Anal. Calcd. for $C_{17}H_{19}ClIrNO_4$: C, 38.58; H, 3.62; N, 2.65. Found: C, 38.90; H, 3.80; N, 2.46.

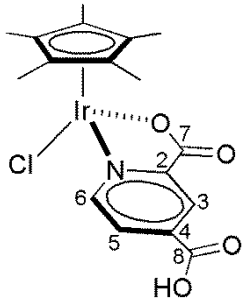

^{1}H NMR (0.4 mL DMSO-d_6 + 0.1mL D_2O (pH = 1 by HNO_3), 298K, 400.13 MHz): δ 8.96 (d, $^{3}J_{HH}$ = 5.6, 1H, H6), 8.18 (d, $^{4}J_{HH}$ = 1.7, 1H, H3), 8.16 (dd, $^{3}J_{HH}$ = 5.6, $^{4}J_{HH}$ = 1.7, 1H, H5), 1.61 (s, 15H, Cp^*). $^{13}C\{^{1}H\}$ NMR (0.4mL DMSO-d_6 + 0.1 mL D_2O (pH

= 1 by HNO_3)): 172.5 (C7), 165.3 (C8), 152.8 (C6), 152.0 (C2), 141.6 (C4), 129.3 (C5), 126.0 (C3), 86.6 (C-Cp^*), 9.3 (CH_3-Cp^*).

[$Cp^*Ir(\kappa^2$-N,O)Cl] (κ^2-N,O = 2,6-pyridinedicarboxylic acid, ion(-1),) (**3**). [$Cp^*IrCl(\mu$-Cl)]$_2$ (100 mg, 0.126 mmol) and 2.4 equivalents of 2,6-pyridinedicarboxylic acid (50.4 mg, 0.302 mmol) were dissolved in 30 mL of methanol. A standard solution of sodium ethoxide was prepared by reacting an exact amount of sodium metal with ethanol. An aliquot of this solution, containing 0.378 mmol of NaOEt, was added to the reaction mixture at room temperature. In a few minutes, the formation of a precipitate was observed and the solution changed color from orange to yellow. After stirring for 2h at RT, the solution was concentrated under reduced pressure and left at -20°C overnight. Finally the solid was filtered off, washed with cold methanol and dried under reduced pressure (98.6 mg, 74%). Anal. Calcd. for $C_{17}H_{19}ClIrNO_4$: C, 38.58; H, 3.62; N, 2.65. Found: C, 38.75; H, 3.71; N, 2.51.

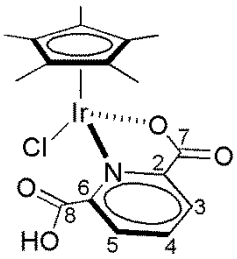

^{1}H NMR (400.13 MHz, CD_2Cl_2): δ = 11.7 (brd, O*H*), 8.31 (dd, 1H, $^3J_{HH}$ = 6.9, $^4J_{HH}$ = 2.5, H3), 8.19 (AB-system, 2H, H5 and H4), 1.59 (s, 15H, Cp^*) ppm. $^{13}C\{^1H\}$ NMR (125.77 MHz, CD_2Cl_2): 171.0 (C7), 165.0 (C8), 152.5, 151.8, 141.2 (C4), 131.4 (C5), 130.1 (C3), 87.5 (C-Cp^*), 9.1 (CH_3-Cp^*) ppm.

[Ir(κ^3-N,O,O)(1-κ-4,5-η^2-C_8H_{13})(MeOH)] (κ^3-N,O,O = 2,6-pyridinedicarboxylic acid, ion(-2)), (**4**). This compound was synthesized in 80-90% overall yield according to the procedure reported in literature.[3] [Ir(μ-OMe)(1-κ-4,5-η^2-C_8H_{13})$_2$]$_2$ (50 mg, 0.075 mmol)

and 2,6-pyridinedicarboxylic acid (25 mg, 0.203 mmol) were reacted in CH_2Cl_2/MeOH mixture (3/1, 10 mL) at room temperature for 14 h. The resulting yellow solution was filtered and then concentrated to dryness under reduced pressure. The crude compound was dissolved in a CH_2Cl_2/MeOH mixture (20:1) mixture (3 mL) and then eluted through an alumina column (7 x 1.5 cm) to give a yellow solution. Concentration of the solution to *ca.* 1 mL and slow addition of diethyl ether gave the compound as a yellow solid which was filtered, washed with diethyl ether (2 x 3 mL) and dried under reduced pressure. ^{1}H and ^{13}C data were identical to those reported in the literature.[3]

X-ray structure determination

A crystal of **3** was mounted on a Bruker APEXII CCD diffractometer and cooled to 180(2)K for the for the unit cell determination and data collection. The space group was unambiguously determined from the systematic absences.

The cell constants were refined by least-squares, at the end of the data collection, using reflections up to $2\theta_{max} \leq 62.5$ deg. The data were collected by using ω scans, in steps of 0.5 deg . For each of the 1440 collected frames, counting time was 20 sec.

The collected intensities were corrected for Lorentz and polarization factors[4] and empirically for absorption using the SADABS program.[5]

Crystal data collection and refinement parameters are listed in Table S1 and in the cif file.

The structure was solved by direct and Fourier methods and refined by full matrix least squares,[6] minimizing the function $[\Sigma w(F_o^2 - (1/k)F_c^2)2]$ using anisotropic displacement parameters for all atoms, except the hydrogens.

The H atom of the carboxylic group, involved in the strong intermolecular hydrogen-bond, was located from a difference-Fourier map and the coordinates refined freely with $B_{iso}(H) = 1.5x\ B(O2)$; the contribution of the remaining hydrogen atoms, in their calculated positions, was included in the refinement using a riding model ($B(H) = 1.5xB(C_{bonded})(Å^2)$).

At the end of the refinement a difference Fourier map showed no significant feature.

Refining the Flack's parameter tested the handedness of the structure.[7]

All calculations and plotting were carried out by using the PC version of SHELX-97,[6] WINGX,[8] ORTEP[8] and Mercury programs.[9]

An ORTEP view of the molecule with the full numbering scheme is given if Figure S1, while the Hydrogen-bond network is shown in Figure S2 and a space filling model is shown in Figure S3.

Extended lists of bond lengths (Å), bond angles (deg) and torsion angles (deg) are given in Tables S2 and S3 while atomic coordinates and displacement parameters are listed in the cif file.

Table S1. Experimental and data refinement for the X-ray Diffraction Study of Compound **3.**

formula	$C_{17}H_{19}ClIrNO_4$
fw	528.98
data coll. *T*, K	180 (2)
cryst syst	Orthorhombic
space group (no.)	$P2_12_12_1$ (19)
a, Å	7.4750(6)
b, Å	14.064(1)
c, Å	15.943(1)
V, Å^3	1676.0(2)
Z	4
$\rho_{(calcd)}$, g cm^{-3}	2.096
μ, cm^{-1}	81.47
radiation	MoKα (graph. mon., λ = 0.71073 Å)
θ range, deg	$2.56 < \theta < 31.52$
no. data collected	26130
no. independent data	5283
no. obs. Reflections (n_o) [$\|F_o\|^2 > 2.0\sigma(\|F\|^2)$]	5020
no. of param. refined (n_v)	220
R_{int}	0.0329
R (obsd reflns)[a]	0.0163
R^2_w (obsd reflns) [b]	0.0351
R (all data)[a]	0.0187
R^2_w (all data) [b]	0.0358
GOF [c]	1.044

[b] $R = \Sigma (|F_o - (1/k) F_c|) / \Sigma|F_o|$ [c] $R^2_w = \{\Sigma [w(F_o^2 - (1/k)F_c^2)^2] / \Sigma w|F_o^2|^2]\}^{1/2}$

[d] GOF = $[\Sigma_w (F_o^2 - (1/k) F_c^2)^2 / (n_o - n_v)]^{1/2}$

Table S2. Bond lengths [Å] and angles [deg] for **3**.

Ir-O(4)	2.1079(18)	C(7)-O(1)	1.192(3)
Ir-C(13)	2.141(3)	C(7)-O(2)	1.328(3)
Ir-N(1)	2.147(2)	C(8)-O(3)	1.207(4)
Ir-C(11)	2.149(3)	C(8)-O(4)	1.287(3)
Ir-C(12)	2.149(3)	O(2)-H(1O)	0.81(4)
Ir-C(14)	2.151(3)	C(11)-C(15)	1.439(4)
Ir-C(15)	2.169(3)	C(11)-C(12)	1.443(4)
Ir-Cl	2.3956(7)	C(11)-C(16)	1.484(4)
N(1)-C(2)	1.340(3)	C(12)-C(13)	1.425(4)
N(1)-C(6)	1.367(3)	C(12)-C(17)	1.497(4)
C(2)-C(3)	1.393(4)	C(13)-C(14)	1.456(4)
C(2)-C(8)	1.520(4)	C(13)-C(18)	1.491(4)
C(3)-C(4)	1.377(4)	C(14)-C(15)	1.433(4)
C(4)-C(5)	1.387(4)	C(14)-C(19)	1.487(4)
C(5)-C(6)	1.384(4)	C(15)-C(110)	1.491(4)
C(6)-C(7)	1.498(4)		

O(4)-Ir-C(13)	115.54(9)	C(11)-Ir-C(14)	66.00(10)
O(4)-Ir-N(1)	76.67(7)	C(12)-Ir-C(14)	65.51(10)
C(13)-Ir-N(1)	167.28(9)	O(4)-Ir-C(15)	143.08(9)
O(4)-Ir-C(11)	105.28(9)	C(13)-Ir-C(15)	65.24(10)
C(13)-Ir-C(11)	66.00(10)	N(1)-Ir-C(15)	103.05(9)
N(1)-Ir-C(11)	108.52(9)	C(11)-Ir-C(15)	38.94(11)
O(4)-Ir-C(12)	92.69(9)	C(12)-Ir-C(15)	64.72(11)
C(13)-Ir-C(12)	38.79(10)	C(14)-Ir-C(15)	38.73(10)
N(1)-Ir-C(12)	142.49(9)	O(4)-Ir-Cl	83.67(6)
C(11)-Ir-C(12)	39.23(9)	C(13)-Ir-Cl	96.43(8)
O(4)-Ir-C(14)	155.08(9)	N(1)-Ir-Cl	88.22(6)
C(13)-Ir-C(14)	39.65(10)	C(11)-Ir-Cl	162.31(7)
N(1)-Ir-C(14)	127.92(10)	C(12)-Ir-Cl	126.79(7)

C(14)-Ir-Cl	99.45(8)	C(11)-C(12)-Ir	70.38(14)

C(15)-Ir-Cl	133.15(8)	C(17)-C(12)-Ir	124.68(19)
C(2)-N(1)-C(6)	117.6(2)	C(12)-C(13)-C(14)	107.8(2)
C(2)-N(1)-Ir	113.65(17)	C(12)-C(13)-C(18)	126.9(3)
C(6)-N(1)-Ir	128.58(17)	C(14)-C(13)-C(18)	125.3(3)
N(1)-C(2)-C(3)	123.2(3)	C(12)-C(13)-Ir	70.92(15)
N(1)-C(2)-C(8)	116.1(2)	C(14)-C(13)-Ir	70.56(15)
C(3)-C(2)-C(8)	120.6(2)	C(18)-C(13)-Ir	125.3(2)
C(4)-C(3)-C(2)	119.0(3)	C(15)-C(14)-C(13)	107.1(2)
C(3)-C(4)-C(5)	118.4(2)	C(15)-C(14)-C(19)	127.8(3)
C(4)-C(5)-C(6)	120.1(3)	C(13)-C(14)-C(19)	125.0(3)
N(1)-C(6)-C(5)	121.6(2)	C(15)-C(14)-Ir	71.31(15)
N(1)-C(6)-C(7)	119.0(2)	C(13)-C(14)-Ir	69.79(15)
C(5)-C(6)-C(7)	119.0(2)	C(19)-C(14)-Ir	127.3(2)
O(1)-C(7)-O(2)	124.5(3)	C(14)-C(15)-C(11)	109.3(2)
O(1)-C(7)-C(6)	123.5(2)	C(14)-C(15)-C(110)	125.7(3)
O(2)-C(7)-C(6)	111.9(2)	C(11)-C(15)-C(110)	124.8(3)
O(3)-C(8)-O(4)	126.0(3)	C(14)-C(15)-Ir	69.96(15)
O(3)-C(8)-C(2)	119.8(3)	C(11)-C(15)-Ir	69.78(15)
O(4)-C(8)-C(2)	114.2(2)	C(110)-C(15)-Ir	130.8(2)
C(7)-O(2)-H(1O)	115(3)		
C(8)-O(4)-Ir	118.47(17)		
C(15)-C(11)-C(12)	106.6(2)		
C(15)-C(11)-C(16)	126.5(3)		
C(12)-C(11)-C(16)	126.5(3)		
C(15)-C(11)-Ir	71.29(15)		
C(12)-C(11)-Ir	70.40(14)		
C(16)-C(11)-Ir	128.52(19)		
C(13)-C(12)-C(11)	109.1(2)		
C(13)-C(12)-C(17)	127.0(3)		
C(11)-C(12)-C(17)	123.9(3)		
C(13)-C(12)-Ir	70.29(14)		

Table S3. Torsion angles [deg] for **3**

O(4)-Ir-N(1)-C(2)	8.57(17)	C(15)-Ir-O(4)-C(8)	88.9(3)
C(13)-Ir-N(1)-C(2)	-155.7(4)	Cl-Ir-O(4)-C(8)	-94.8(2)
C(11)-Ir-N(1)-C(2)	-93.33(19)	O(4)-Ir-C(11)-C(15)	-168.71(14)
C(12)-Ir-N(1)-C(2)	-68.2(2)	C(13)-Ir-C(11)-C(15)	79.71(16)
C(14)-Ir-N(1)-C(2)	-166.91(17)	N(1)-Ir-C(11)-C(15)	-87.95(15)
C(15)-Ir-N(1)-C(2)	-133.48(18)	C(12)-Ir-C(11)-C(15)	116.2(2)
Cl-Ir-N(1)-C(2)	92.48(17)	C(14)-Ir-C(11)-C(15)	36.13(15)
O(4)-Ir-N(1)-C(6)	-176.9(2)	Cl-Ir-C(11)-C(15)	72.6(3)
C(13)-Ir-N(1)-C(6)	18.8(6)	O(4)-Ir-C(11)-C(12)	75.07(16)
C(11)-Ir-N(1)-C(6)	81.2(2)	C(13)-Ir-C(11)-C(12)	-36.50(15)
C(12)-Ir-N(1)-C(6)	106.3(2)	N(1)-Ir-C(11)-C(12)	155.84(15)
C(14)-Ir-N(1)-C(6)	7.6(3)	C(14)-Ir-C(11)-C(12)	-80.08(17)
C(15)-Ir-N(1)-C(6)	41.0(2)	C(15)-Ir-C(11)-C(12)	-116.2(2)
Cl-Ir-N(1)-C(6)	-93.0(2)	Cl-Ir-C(11)-C(12)	-43.6(3)
C(6)-N(1)-C(2)-C(3)	-2.3(4)	O(4)-Ir-C(11)-C(16)	-46.5(3)
Ir-N(1)-C(2)-C(3)	172.8(2)	C(13)-Ir-C(11)-C(16)	-158.0(3)
C(6)-N(1)-C(2)-C(8)	174.1(2)	N(1)-Ir-C(11)-C(16)	34.3(3)
Ir-N(1)-C(2)-C(8)	-10.8(3)	C(12)-Ir-C(11)-C(16)	-121.5(4)
N(1)-C(2)-C(3)-C(4)	-1.2(4)	C(14)-Ir-C(11)-C(16)	158.4(3)
C(8)-C(2)-C(3)-C(4)	-177.4(3)	C(15)-Ir-C(11)-C(16)	122.2(3)
C(2)-C(3)-C(4)-C(5)	2.7(4)	Cl-Ir-C(11)-C(16)	-165.2(2)
C(3)-C(4)-C(5)-C(6)	-0.8(5)	C(15)-C(11)-C(12)-C(13)	-2.7(3)
C(2)-N(1)-C(6)-C(5)	4.3(4)	C(16)-C(11)-C(12)-C(13)	-176.2(2)
Ir-N(1)-C(6)-C(5)	-170.0(2)	Ir-C(11)-C(12)-C(13)	59.81(18)
C(2)-N(1)-C(6)-C(7)	-168.0(2)	C(15)-C(11)-C(12)-C(17)	178.3(2)
Ir-N(1)-C(6)-C(7)	17.7(3)	C(16)-C(11)-C(12)-C(17)	4.7(4)
C(4)-C(5)-C(6)-N(1)	-2.8(4)	Ir-C(11)-C(12)-C(17)	-119.2(3)
C(4)-C(5)-C(6)-C(7)	169.5(3)	C(15)-C(11)-C(12)-Ir	-62.49(18)
N(1)-C(6)-C(7)-O(1)	37.6(4)	C(16)-C(11)-C(12)-Ir	124.0(3)
C(5)-C(6)-C(7)-O(1)	-135.0(3)	O(4)-Ir-C(12)-C(13)	129.09(15)
N(1)-C(6)-C(7)-O(2)	-146.6(2)	N(1)-Ir-C(12)-C(13)	-159.44(15)
C(5)-C(6)-C(7)-O(2)	40.9(3)	C(11)-Ir-C(12)-C(13)	-119.8(2)
N(1)-C(2)-C(8)-O(3)	-171.6(3)	C(14)-Ir-C(12)-C(13)	-38.39(16)
C(3)-C(2)-C(8)-O(3)	4.9(5)	C(15)-Ir-C(12)-C(13)	-81.27(16)
N(1)-C(2)-C(8)-O(4)	6.6(4)	Cl-Ir-C(12)-C(13)	44.98(17)
C(3)-C(2)-C(8)-O(4)	-176.9(3)	O(4)-Ir-C(12)-C(11)	-111.07(15)
O(3)-C(8)-O(4)-Ir	179.3(3)	C(13)-Ir-C(12)-C(11)	119.8(2)
C(2)-C(8)-O(4)-Ir	1.2(3)	N(1)-Ir-C(12)-C(11)	-39.6(2)
C(13)-Ir-O(4)-C(8)	171.0(2)	C(14)-Ir-C(12)-C(11)	81.45(17)
N(1)-Ir-O(4)-C(8)	-5.2(2)	C(15)-Ir-C(12)-C(11)	38.58(16)
C(11)-Ir-O(4)-C(8)	100.7(2)	Cl-Ir-C(12)-C(11)	164.82(12)
C(12)-Ir-O(4)-C(8)	138.4(2)	O(4)-Ir-C(12)-C(17)	7.1(2)
C(14)-Ir-O(4)-C(8)	166.3(3)	C(13)-Ir-C(12)-C(17)	-122.0(3)
		N(1)-Ir-C(12)-C(17)	78.6(3)

C(11)-Ir-C(12)-C(17)	118.2(3)
C(14)-Ir-C(12)-C(17)	-160.4(3)
C(15)-Ir-C(12)-C(17)	156.8(3)
Cl-Ir-C(12)-C(17)	-77.0(3)
C(11)-C(12)-C(13)-C(14)	1.4(3)
C(17)-C(12)-C(13)-C(14)	-179.6(3)
Ir-C(12)-C(13)-C(14)	61.28(18)
C(11)-C(12)-C(13)-C(18)	179.8(3)
C(17)-C(12)-C(13)-C(18)	-1.2(4)
Ir-C(12)-C(13)-C(18)	-120.3(3)
C(11)-C(12)-C(13)-Ir	-59.87(18)
C(17)-C(12)-C(13)-Ir	119.1(3)
O(4)-Ir-C(13)-C(12)	-59.24(17)
N(1)-Ir-C(13)-C(12)	103.8(4)
C(11)-Ir-C(13)-C(12)	36.90(15)
C(14)-Ir-C(13)-C(12)	117.7(2)
C(15)-Ir-C(13)-C(12)	79.82(17)
Cl-Ir-C(13)-C(12)	-145.28(14)
O(4)-Ir-C(13)-C(14)	-176.90(15)
N(1)-Ir-C(13)-C(14)	-13.9(5)
C(11)-Ir-C(13)-C(14)	-80.76(17)
C(12)-Ir-C(13)-C(14)	-117.7(2)
C(15)-Ir-C(13)-C(14)	-37.84(16)
Cl-Ir-C(13)-C(14)	97.07(15)
O(4)-Ir-C(13)-C(18)	63.0(3)
N(1)-Ir-C(13)-C(18)	-134.0(4)
C(11)-Ir-C(13)-C(18)	159.2(3)
C(12)-Ir-C(13)-C(18)	122.3(3)
C(14)-Ir-C(13)-C(18)	-120.1(3)
C(15)-Ir-C(13)-C(18)	-157.9(3)
Cl-Ir-C(13)-C(18)	-23.0(3)
C(12)-C(13)-C(14)-C(15)	0.4(3)
C(18)-C(13)-C(14)-C(15)	-178.0(3)
Ir-C(13)-C(14)-C(15)	61.93(18)
C(12)-C(13)-C(14)-C(19)	176.4(3)
C(18)-C(13)-C(14)-C(19)	-2.0(4)
Ir-C(13)-C(14)-C(19)	-122.1(3)
C(12)-C(13)-C(14)-Ir	-61.52(18)
C(18)-C(13)-C(14)-Ir	120.0(3)
O(4)-Ir-C(14)-C(15)	-110.4(2)
C(13)-Ir-C(14)-C(15)	-117.1(2)
N(1)-Ir-C(14)-C(15)	59.07(19)
C(11)-Ir-C(14)-C(15)	-36.32(16)
C(12)-Ir-C(14)-C(15)	-79.52(17)
Cl-Ir-C(14)-C(15)	154.23(15)
O(4)-Ir-C(14)-C(13)	6.7(3)
N(1)-Ir-C(14)-C(13)	176.16(14)
C(11)-Ir-C(14)-C(13)	80.77(17)
C(12)-Ir-C(14)-C(13)	37.57(16)
C(15)-Ir-C(14)-C(13)	117.1(2)
Cl-Ir-C(14)-C(13)	-88.68(15)
O(4)-Ir-C(14)-C(19)	125.8(3)
C(13)-Ir-C(14)-C(19)	119.2(3)
N(1)-Ir-C(14)-C(19)	-64.7(3)
C(11)-Ir-C(14)-C(19)	-160.1(3)
C(12)-Ir-C(14)-C(19)	156.7(3)
C(15)-Ir-C(14)-C(19)	-123.7(3)
Cl-Ir-C(14)-C(19)	30.5(3)
C(13)-C(14)-C(15)-C(11)	-2.1(3)
C(19)-C(14)-C(15)-C(11)	-178.0(3)
Ir-C(14)-C(15)-C(11)	58.85(18)
C(13)-C(14)-C(15)-C(110)	172.6(3)
C(19)-C(14)-C(15)-C(110)	-3.3(5)
Ir-C(14)-C(15)-C(110)	-126.5(3)
C(13)-C(14)-C(15)-Ir	-60.94(18)
C(19)-C(14)-C(15)-Ir	123.2(3)
C(12)-C(11)-C(15)-C(14)	2.9(3)
C(16)-C(11)-C(15)-C(14)	176.5(2)
Ir-C(11)-C(15)-C(14)	-58.96(18)
C(12)-C(11)-C(15)-C(110)	-171.8(3)
C(16)-C(11)-C(15)-C(110)	1.8(4)
Ir-C(11)-C(15)-C(110)	126.3(3)
C(12)-C(11)-C(15)-Ir	61.90(18)
C(16)-C(11)-C(15)-Ir	-124.6(3)
O(4)-Ir-C(15)-C(14)	138.90(16)
C(13)-Ir-C(15)-C(14)	38.73(16)
N(1)-Ir-C(15)-C(14)	-136.00(15)
C(11)-Ir-C(15)-C(14)	120.6(2)
C(12)-Ir-C(15)-C(14)	81.72(17)
Cl-Ir-C(15)-C(14)	-36.00(19)
O(4)-Ir-C(15)-C(11)	18.3(2)
C(13)-Ir-C(15)-C(11)	-81.85(16)
N(1)-Ir-C(15)-C(11)	103.42(15)
C(12)-Ir-C(15)-C(11)	-38.86(15)
C(14)-Ir-C(15)-C(11)	-120.6(2)
Cl-Ir-C(15)-C(11)	-156.58(12)
O(4)-Ir-C(15)-C(110)	-100.7(3)
C(13)-Ir-C(15)-C(110)	159.2(3)
N(1)-Ir-C(15)-C(110)	-15.6(3)
C(11)-Ir-C(15)-C(110)	-119.0(4)
C(12)-Ir-C(15)-C(110)	-157.9(3)
C(14)-Ir-C(15)-C(110)	120.4(4)
Cl-Ir-C(15)-C(110)	84.4(3)

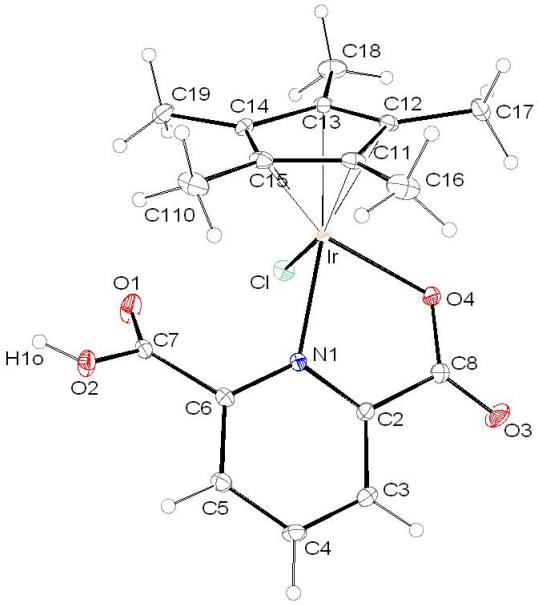

Figure S1. Ortep view of **3** with the full labelling scheme. Elllipsoids are drawn at 50% probability.

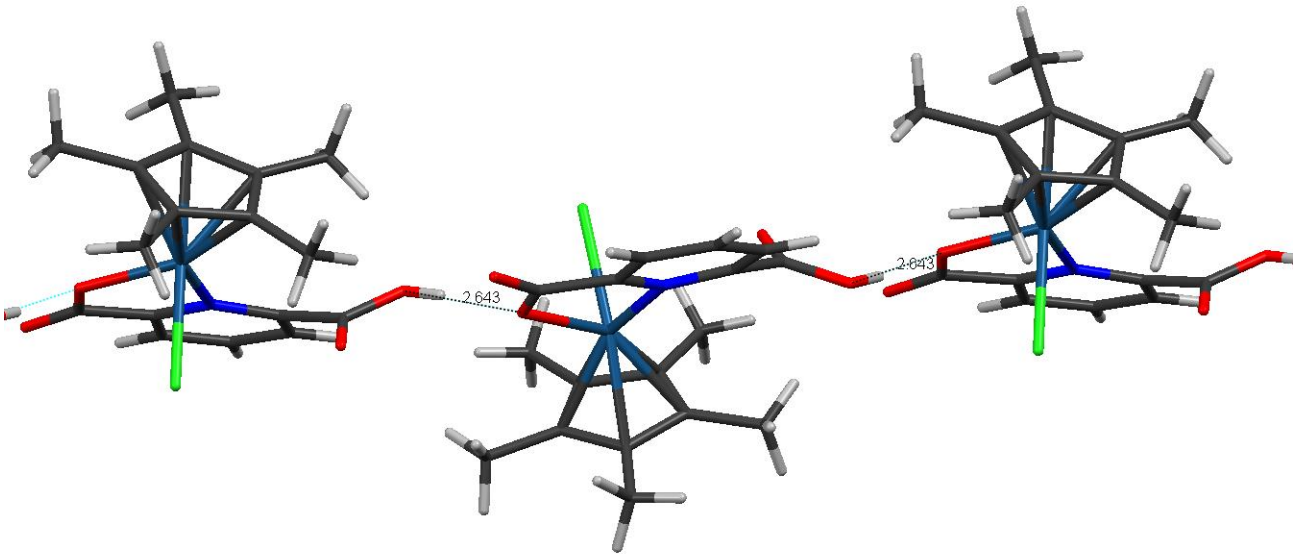

Figure S2. Hydrogen bonding (ligth blu line) between the O2-H groups and O4 of a symmetry related (-x + ½; -y; ½ +z) molecule.

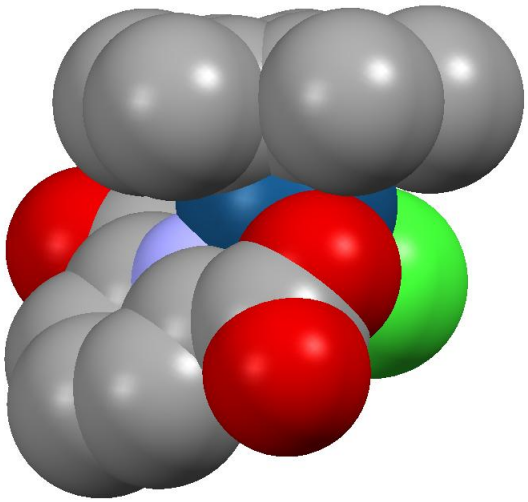

Figure S3. Space filling model of **3**.

Electrochemical measurements

All electrochemical experiments were performed with a Bio-logic SP-150 potentiostat, using a three-electrode cell. A glassy carbon disk (3 mm diameter) from CH Instruments was used as working electrode, a platinum disk (2 mm diameter) from CH Instruments was used as the auxiliary electrode, and a SSCE from BAS was used as the reference electrode. The experiments were carried out in acetonitrile (0.1 M tetrabutylammonium hexafluorophosphate) and in aqueous solutions at different values of pH. pH 1 catalyst solutions were obtained in 0.1 M HNO_3. pH 2, 7 and 11.3 solutions were prepared from different phosphate buffers in which the necessary amount of phosphate salts was used to yield 0.1 M ionic strength solutions.

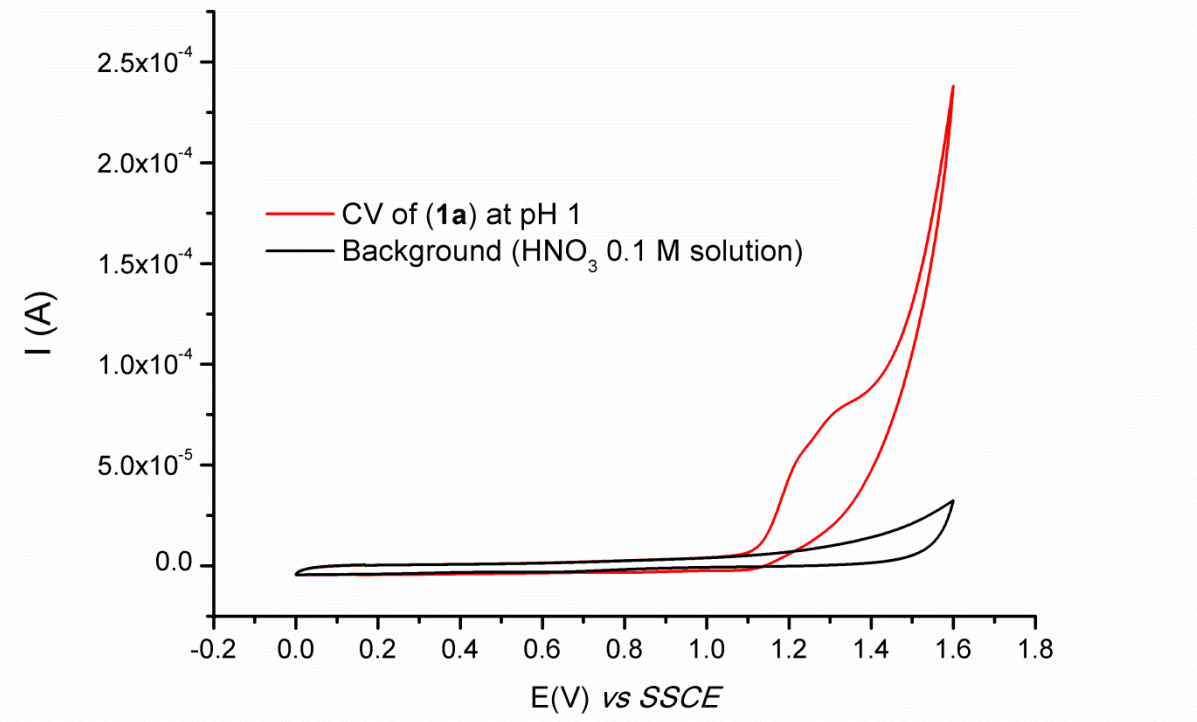

Figure S4. Cyclic voltammetry diagram (scan rate: 50 mV/s) of catalyst **1a** in 0.1 M HNO_3 with a glassy carbon electrode.

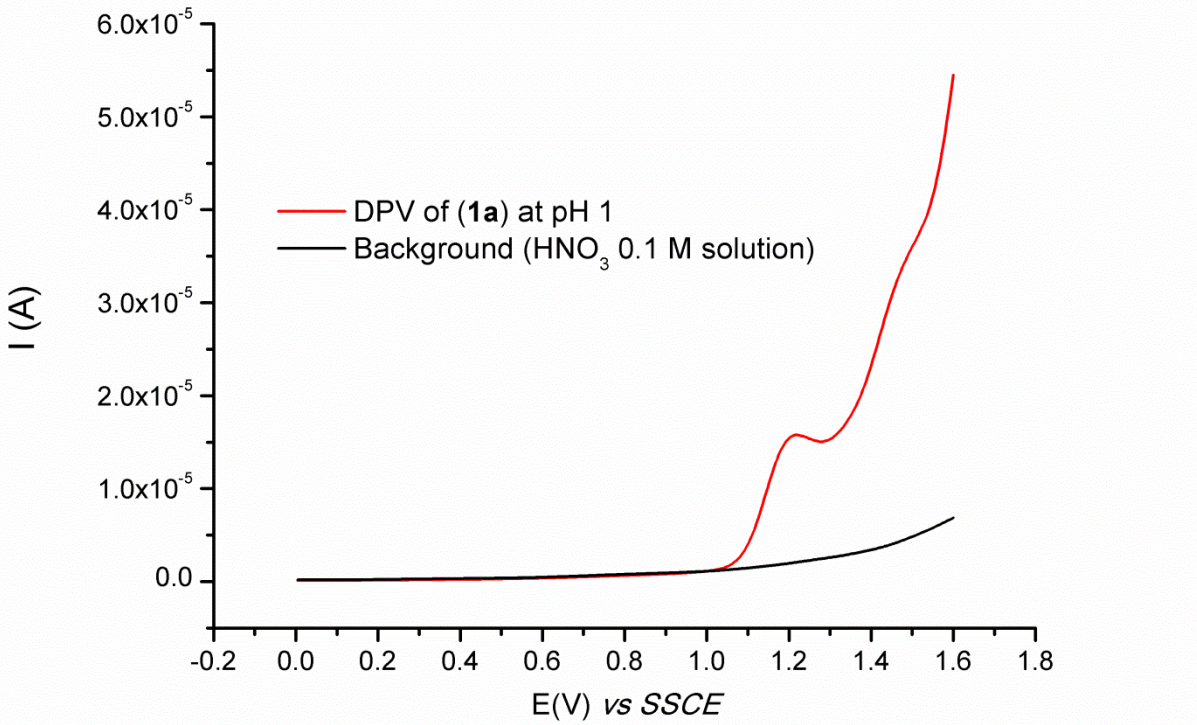

Figure S5. Differential pulse voltammetry diagram of catalyst **1a** in 0.1 M HNO_3 with a glassy carbon electrode.

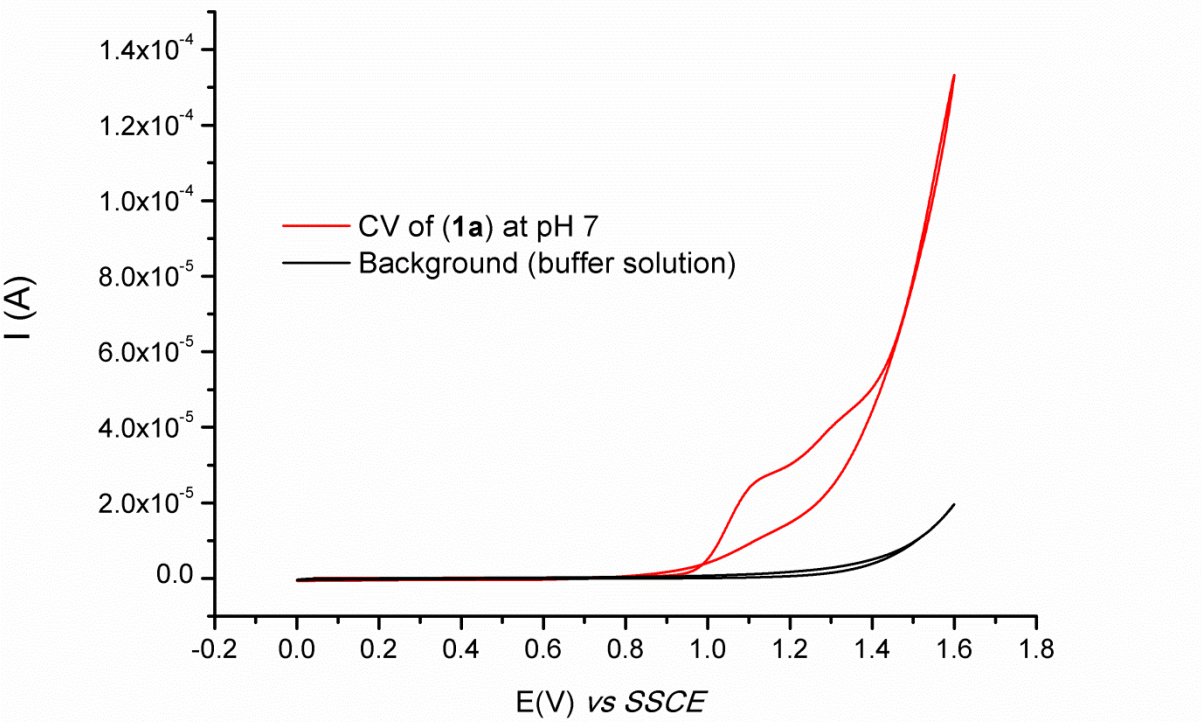

Figure S6. Cyclic voltammetry diagram (scan rate: 10 mV/s) of catalyst **1a** in 0.046 M NaH_2PO_4/Na_2HPO_4 (pH 7) buffer solution with a glassy carbon electrode.

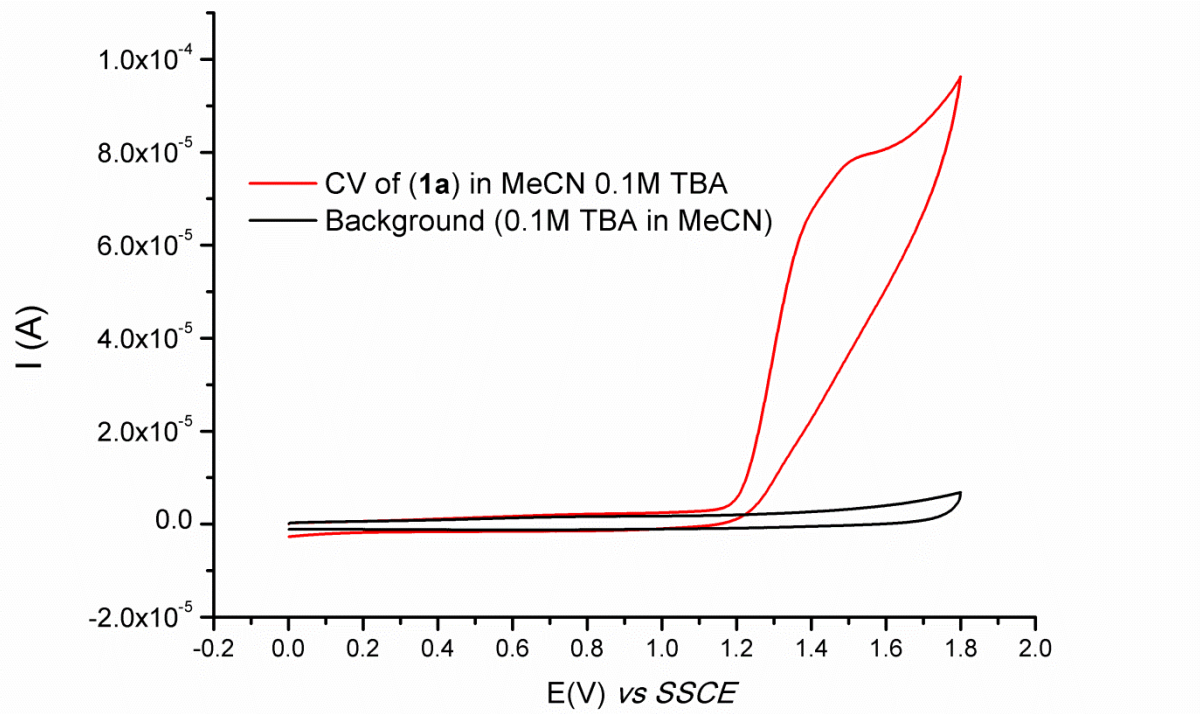

Figure S7. Cyclic voltammetry diagram (scan rate: 100 mV/s) of catalyst **1a** in MeCN 0.1 M TBA (tetrabutylammonium hexafluorophosphate) with a glassy carbon electrode.

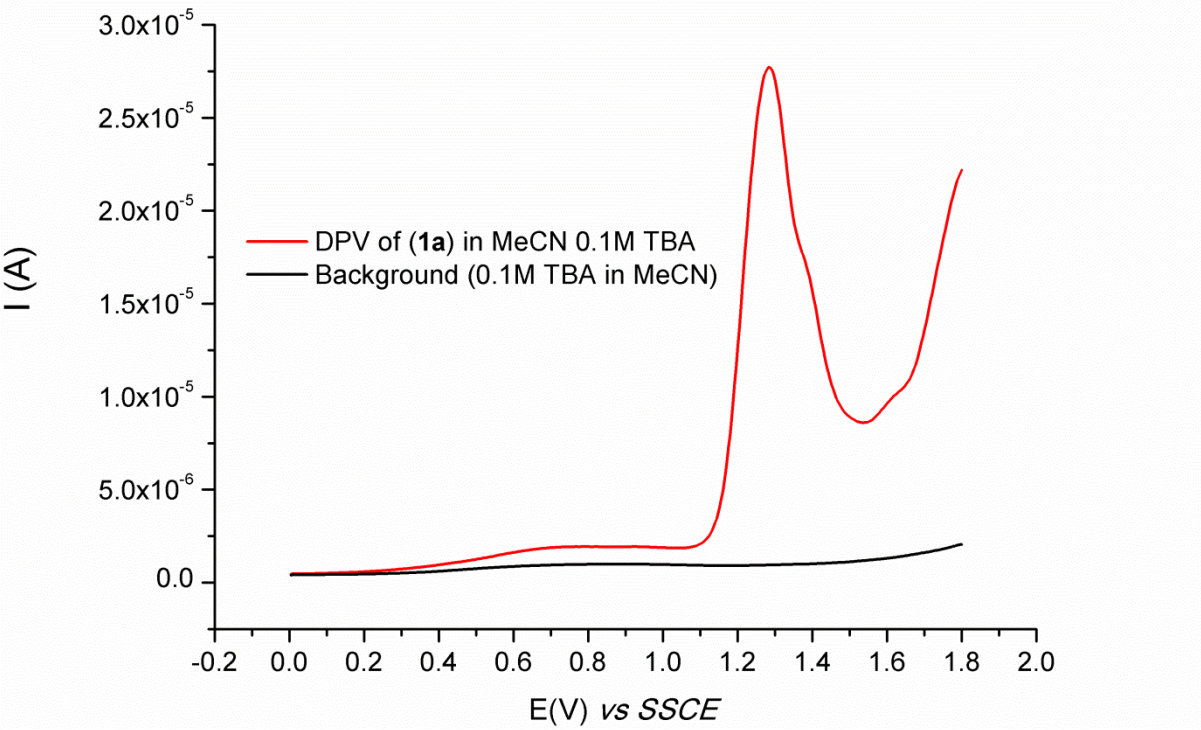

Figure S8. Differential pulse voltammetry diagram of catalyst **1a** in MeCN 0.1 M TBA (tetrabutylammonium hexafluorophosphate) with a glassy carbon electrode.

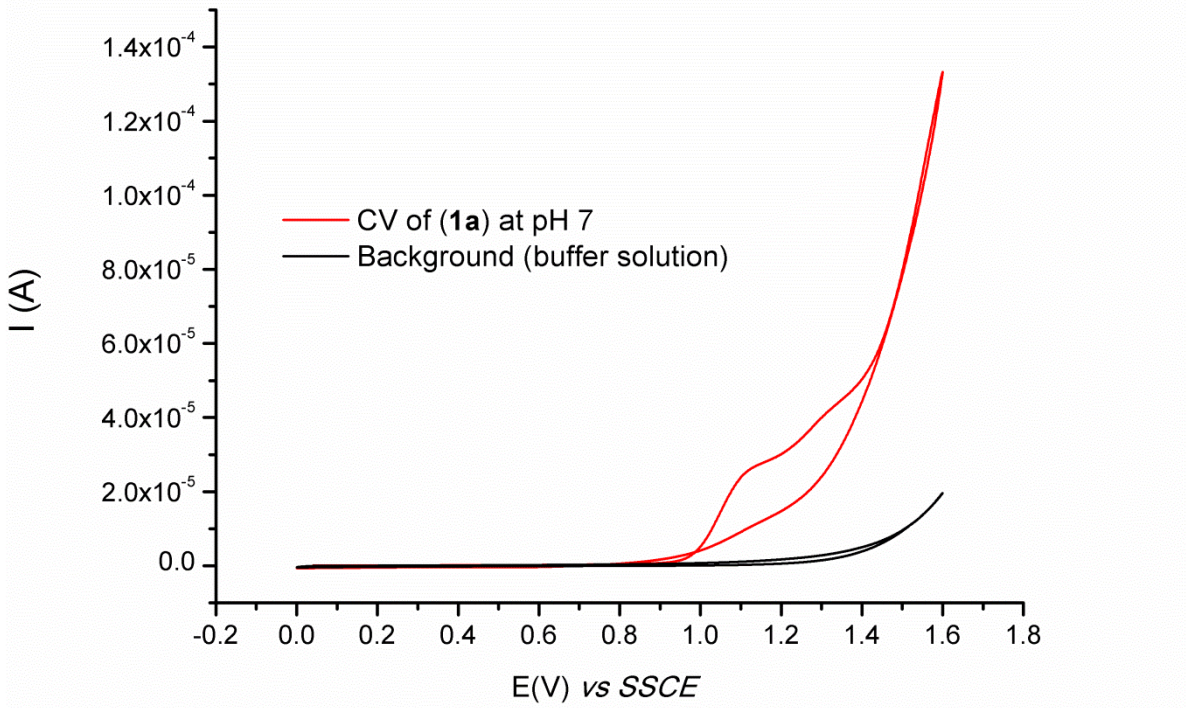

Figure S9. Cyclic voltammetry diagram (scan rate: 100 mV/s) of catalyst **1b** in 0.1 M HNO_3 with a glassy carbon electrode.

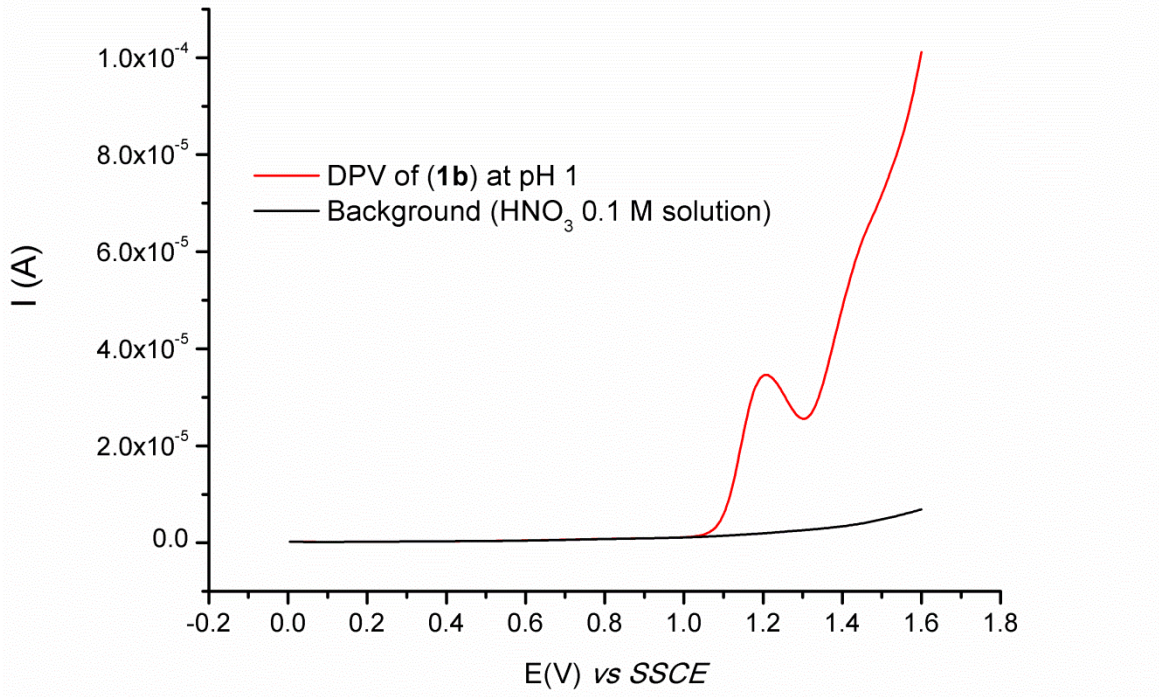

Figure S10. Differential pulse voltammetry diagram of catalyst **1b** in 0.1 M HNO_3 with a glassy carbon electrode.

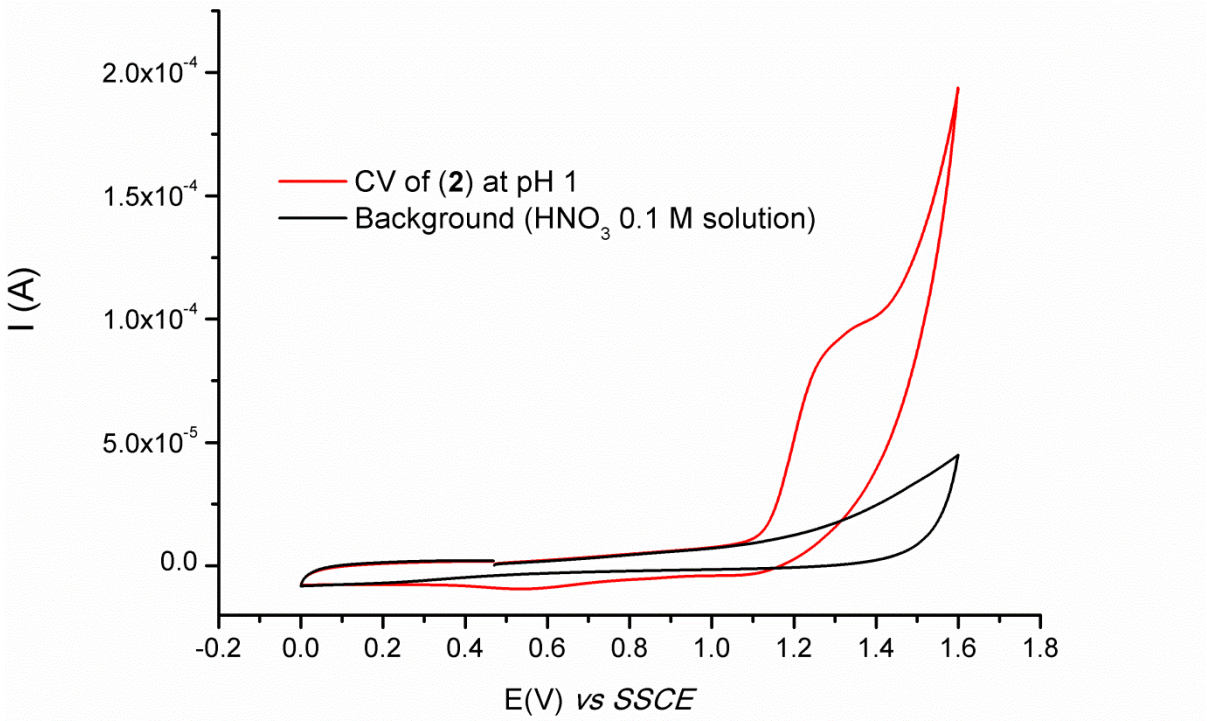

Figure S11. Cyclic voltammetry diagram (scan rate: 100 mV/s) of catalyst **2** in 0.1 M HNO_3 with a glassy carbon electrode.

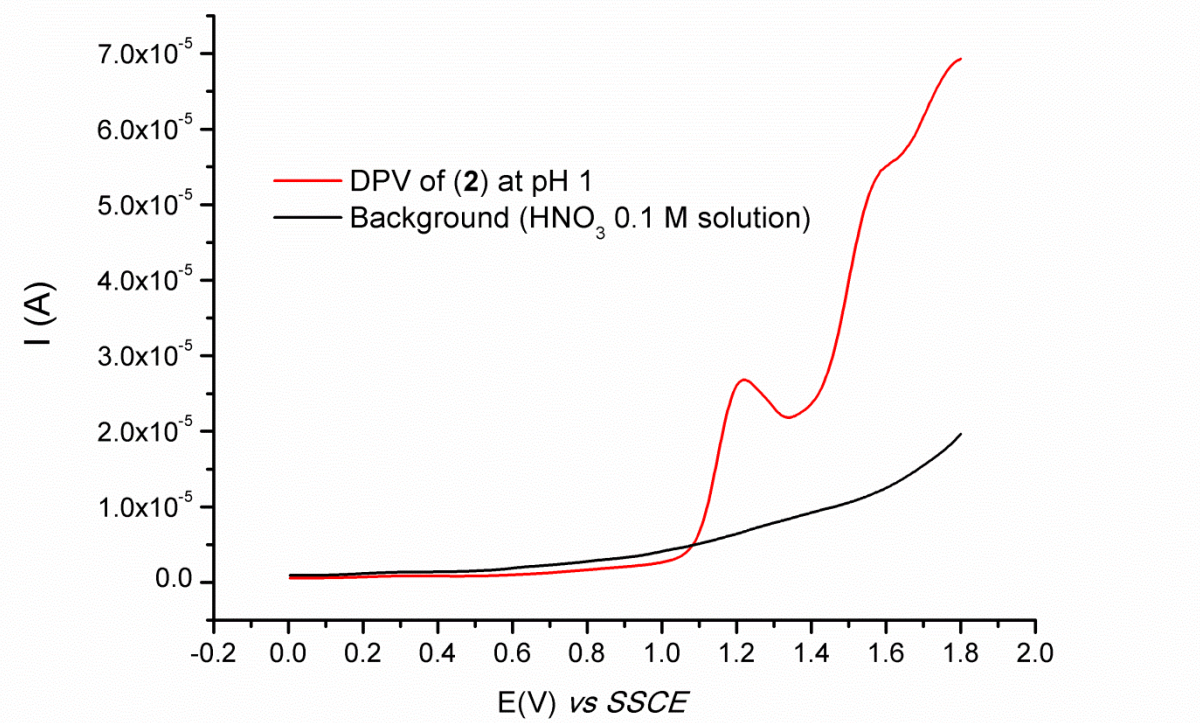

Figure S12. Differential pulse voltammetry diagram of catalyst **2** in 0.1 M HNO_3 with a glassy carbon electrode.

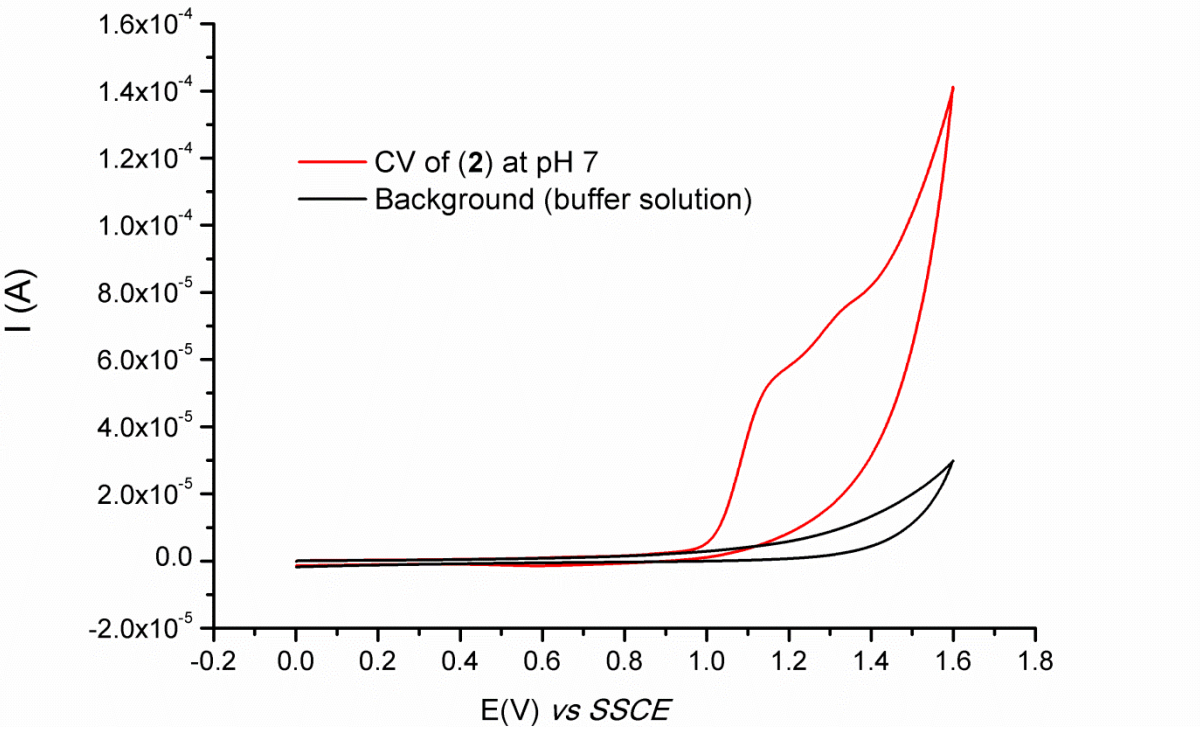

Figure S13. Cyclic voltammetry diagram (scan rate: 50 mV/s) of catalyst **2** in 0.046 M NaH_2PO_4/Na_2HPO_4 (pH 7) buffer solution with a glassy carbon electrode.

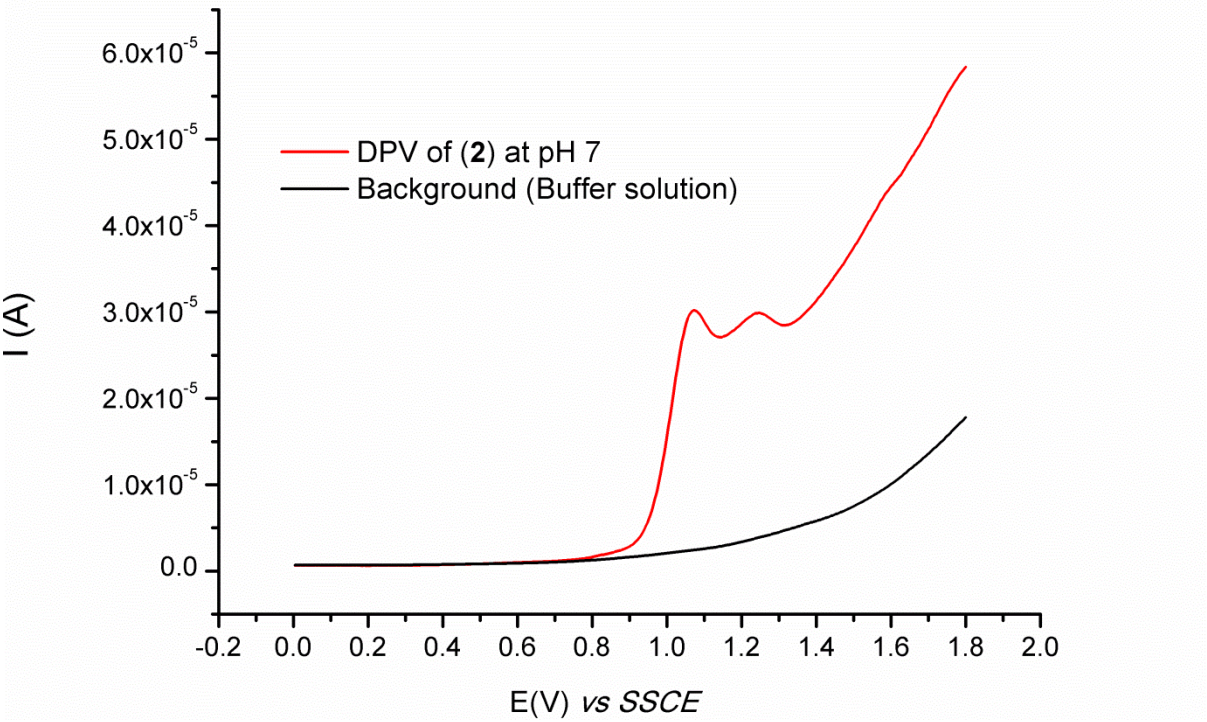

Figure S14. Differential pulse voltammetry diagram of catalyst **2** in 0.046 M NaH_2PO_4/Na_2HPO_4 (pH 7) buffer solution with a glassy carbon electrode.

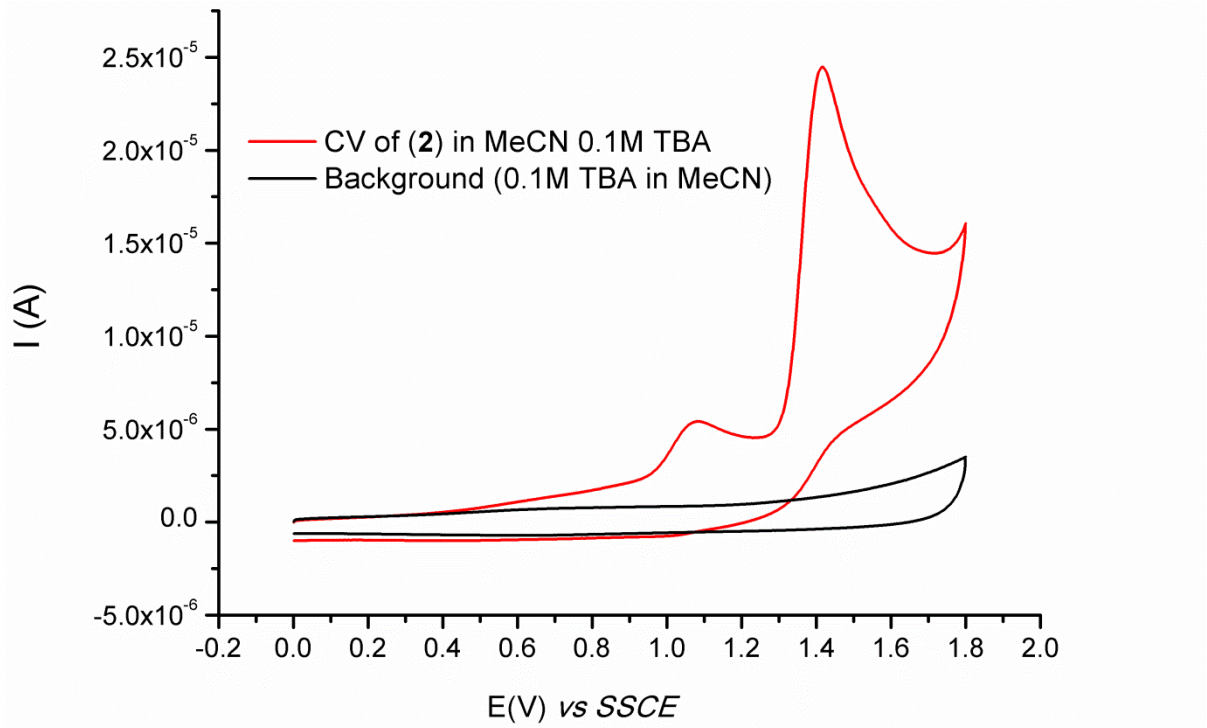

Figure S15. Cyclic voltammetry diagram of catalyst **2** in MeCN 0.1 M TBA (tetrabutylammonium hexafluorophosphate) with a glassy carbon electrode.

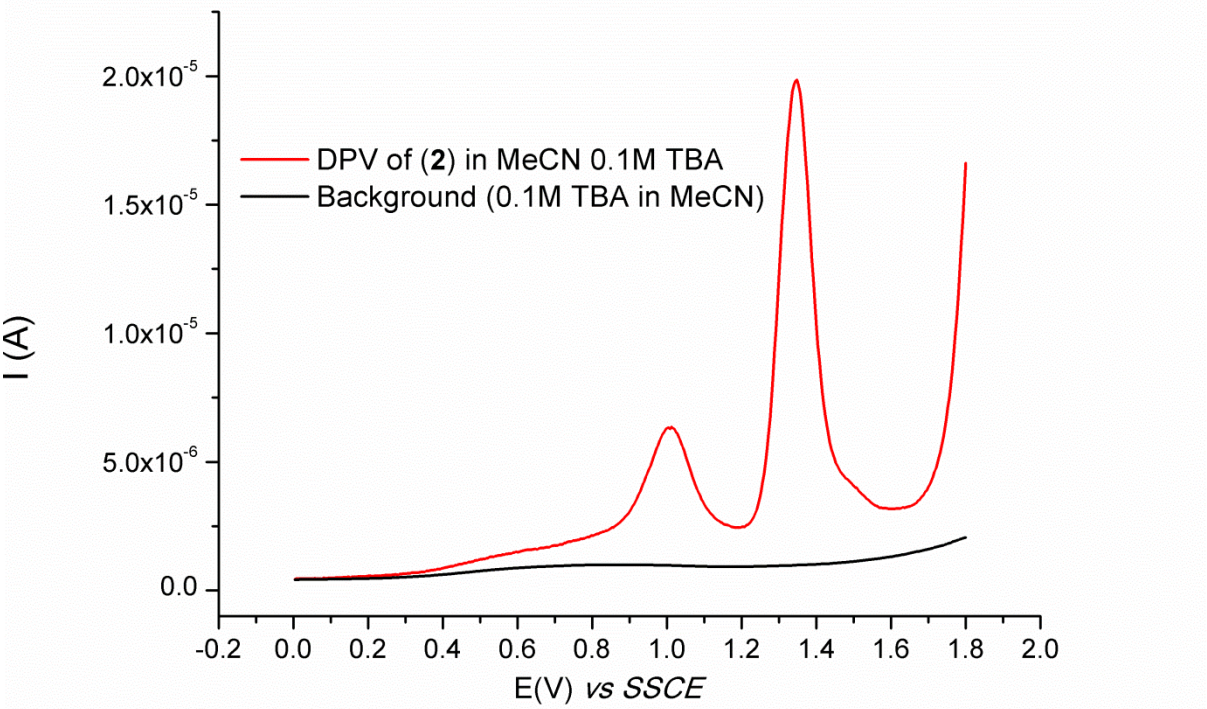

Figure S16. Differential pulse voltammetry diagram of catalyst **2** in MeCN 0.1 M TBA (tetrabutylammonium hexafluorophosphate) with a glassy carbon electrode.

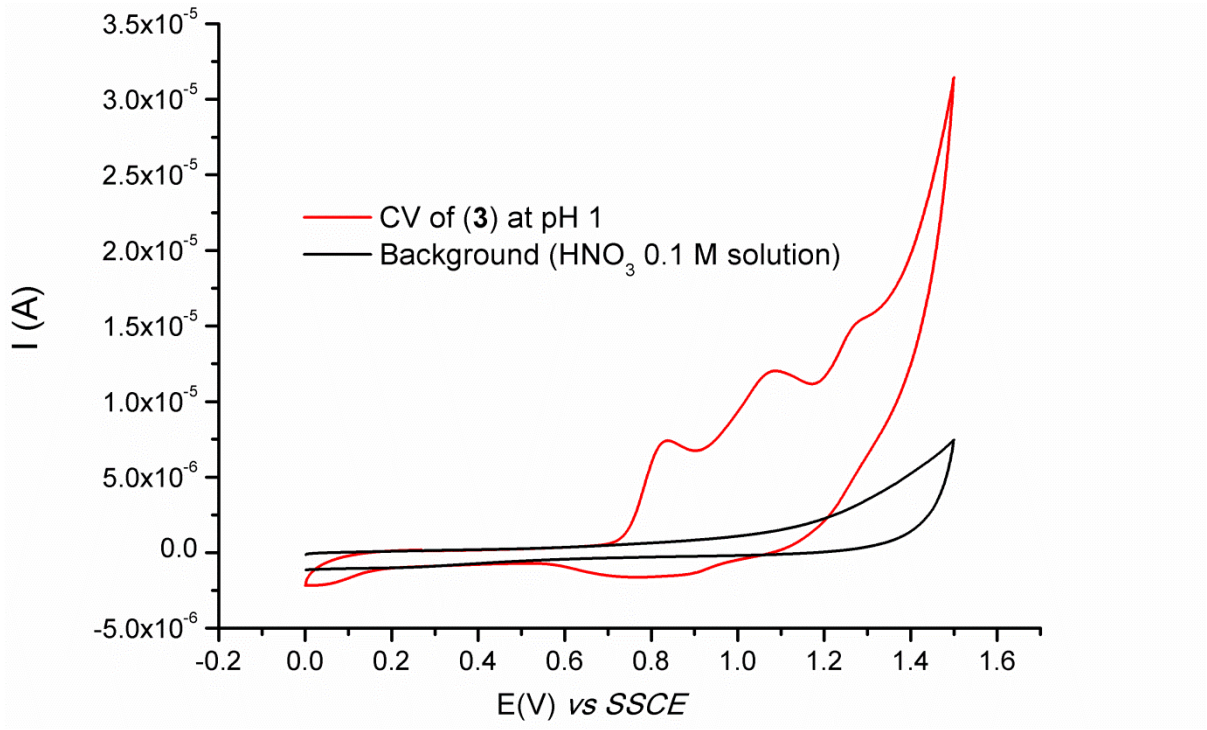

Figure S17. Cyclic voltammetry diagram (scan rate: 10 mV/s) of catalyst **3** in 0.1 M HNO_3 with a glassy carbon electrode.

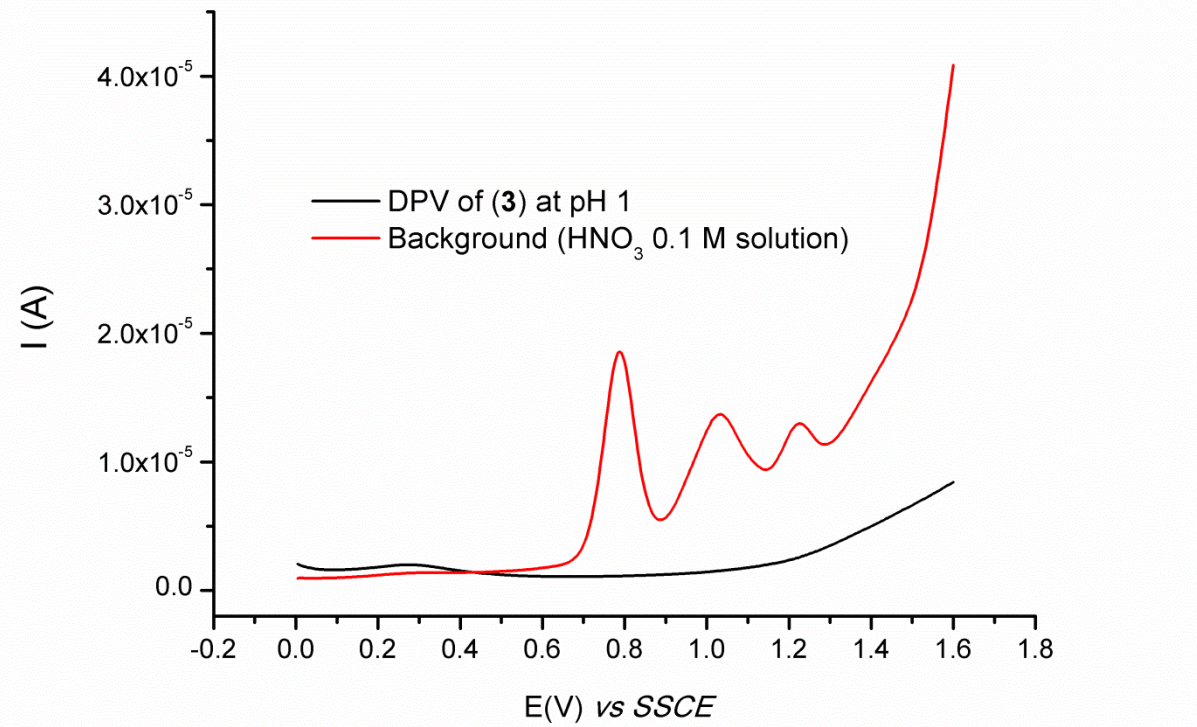

Figure S18. Differential pulse voltammetry diagram of catalyst **3** in 0.1 M HNO_3 with a glassy carbon electrode.

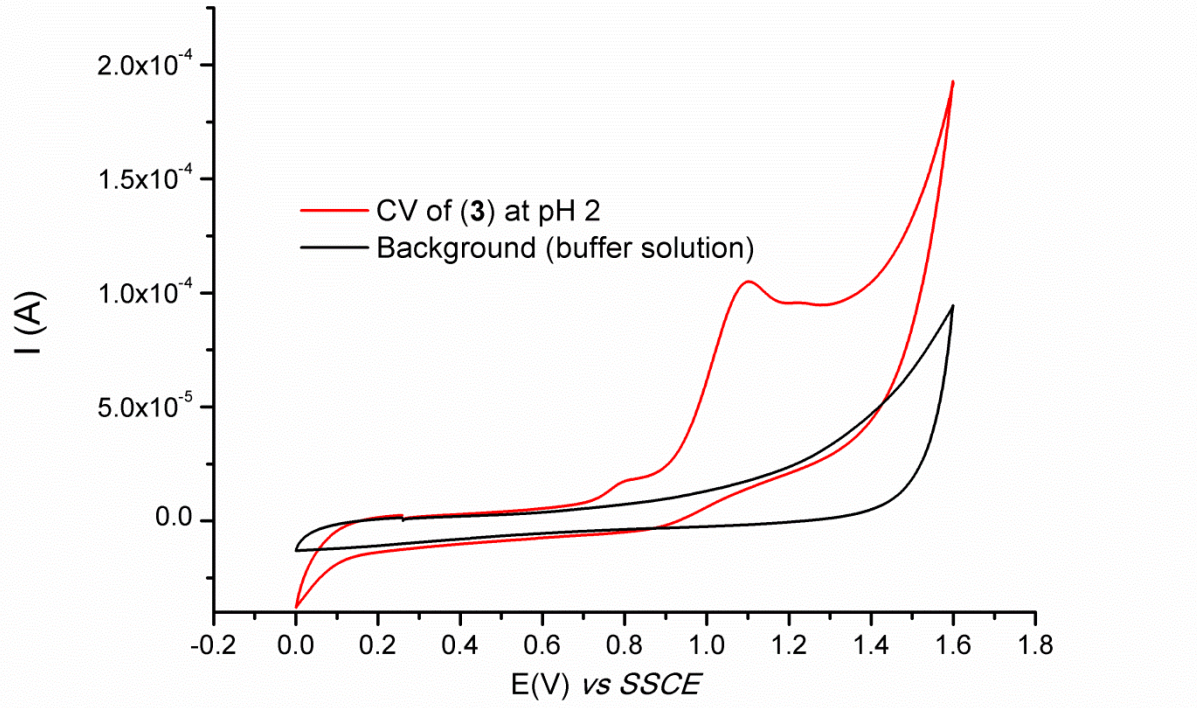

Figure S19. Cyclic voltammetry diagram (scan rate: 500 mV/s) of catalyst **3** in 0.208 M H_3PO_4/ NaH_2PO_4 (pH = 2.04) buffer solution with a glassy carbon electrode.

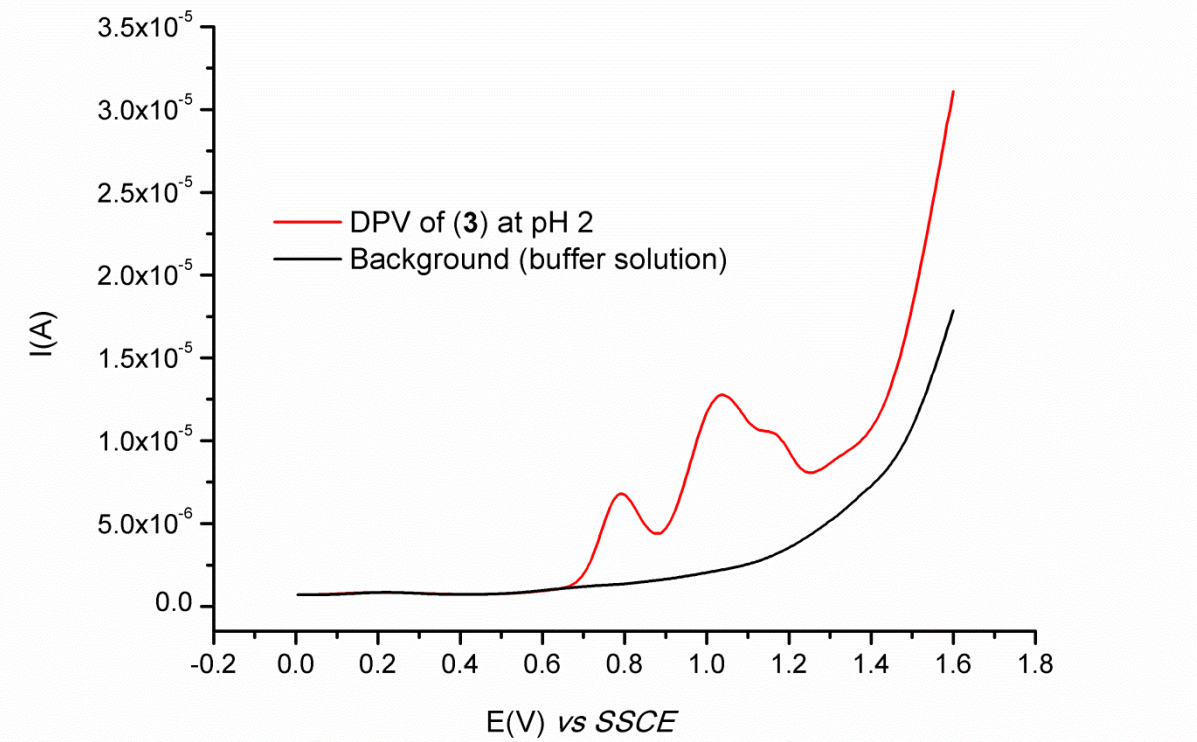

Figure S20. Differential pulse voltammetry diagram of catalyst **3** in 0.208 M H_3PO_4/ NaH_2PO_4 (pH = 2.04) buffer solution with a glassy carbon electrode.

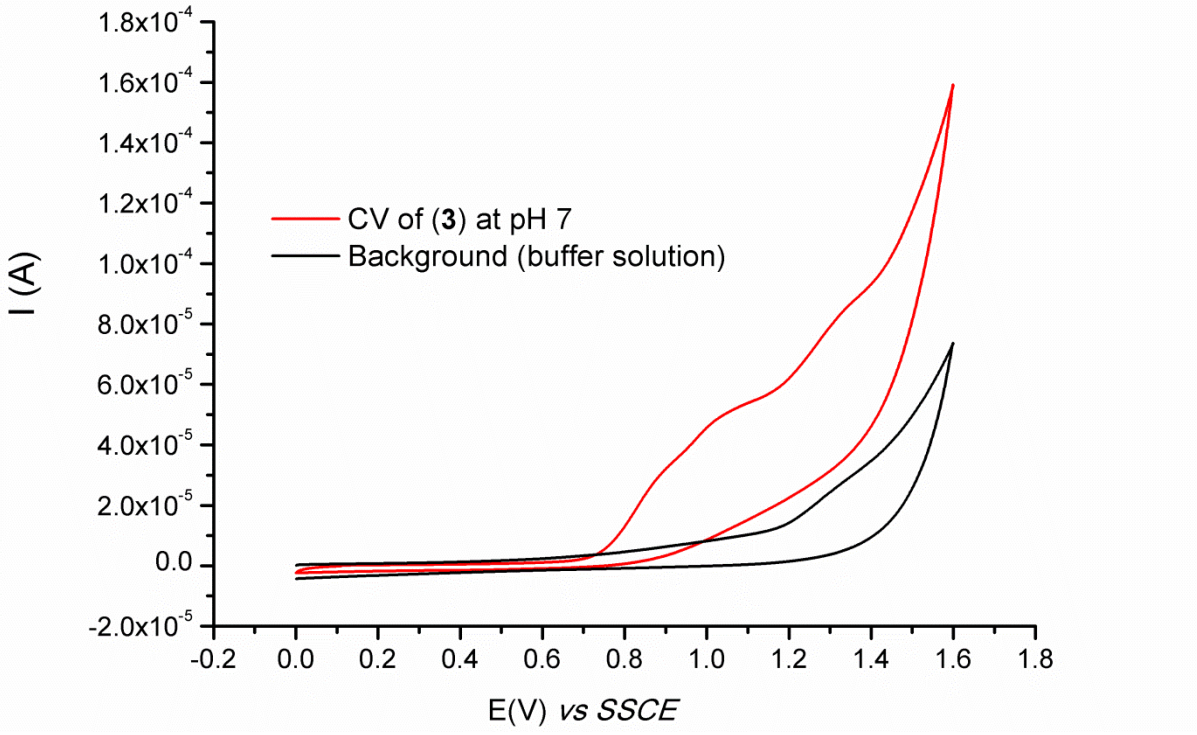

Figure S21. Cyclic voltammetry diagram (scan rate: 100 mV/s) of catalyst **3** in 0.046 M NaH_2PO_4/Na_2HPO_4 (pH 7) buffer solution with a glassy carbon electrode.

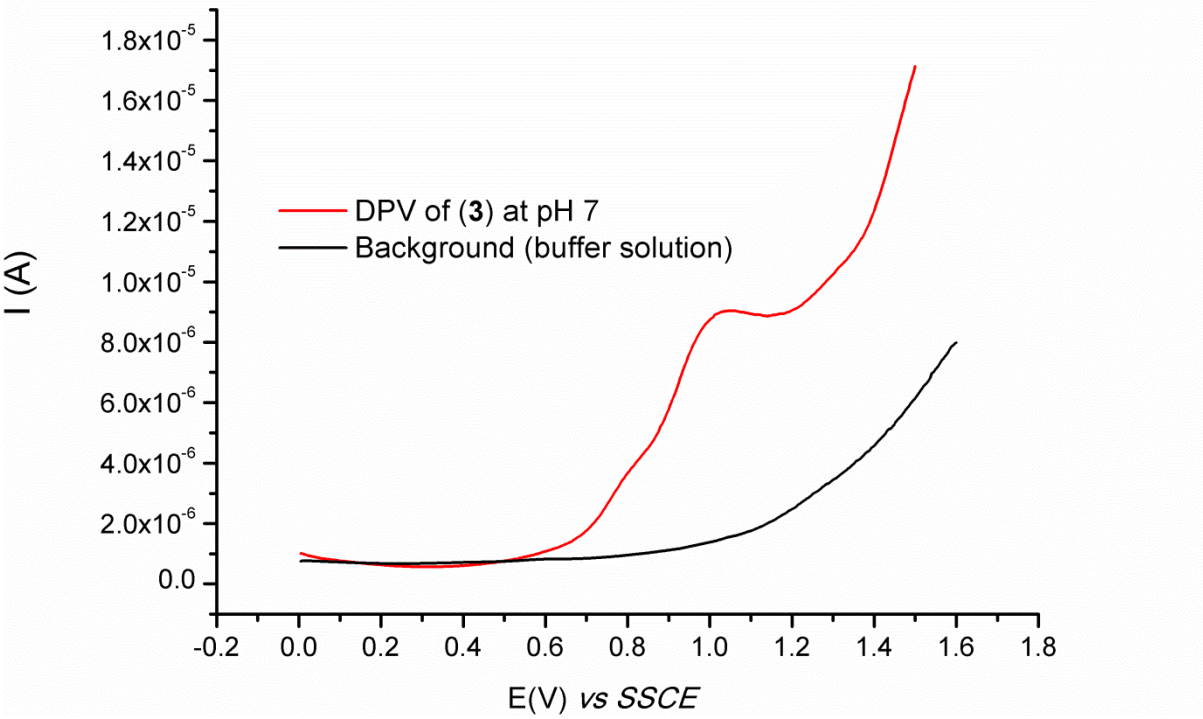

Figure S22. Differential pulse voltammetry diagram of catalyst **3** in 0.046 M NaH_2PO_4/Na_2HPO_4 (pH 7) buffer solution with a glassy carbon electrode.

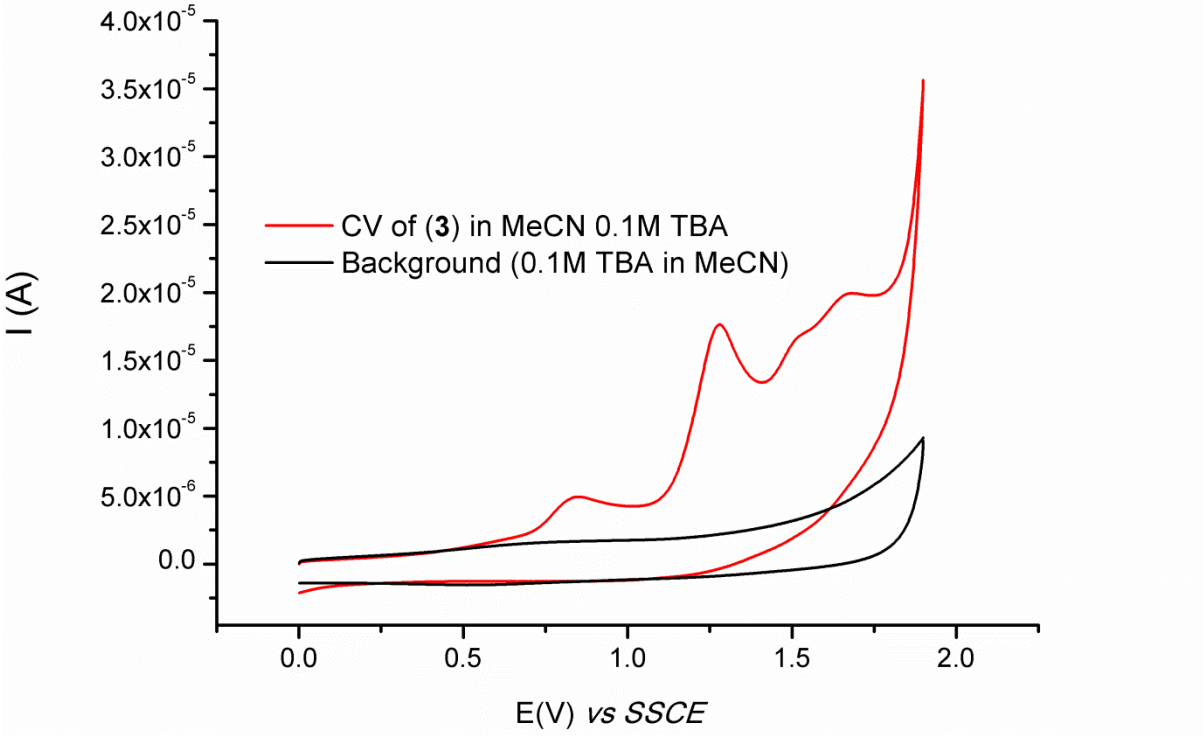

Figure S23. Cyclic voltammetry diagram (scan rate: 100mV/s) of catalyst **3** in MeCN 0.1 M TBA (tetrabutylammonium hexafluorophosphate) with a glassy carbon electrode.

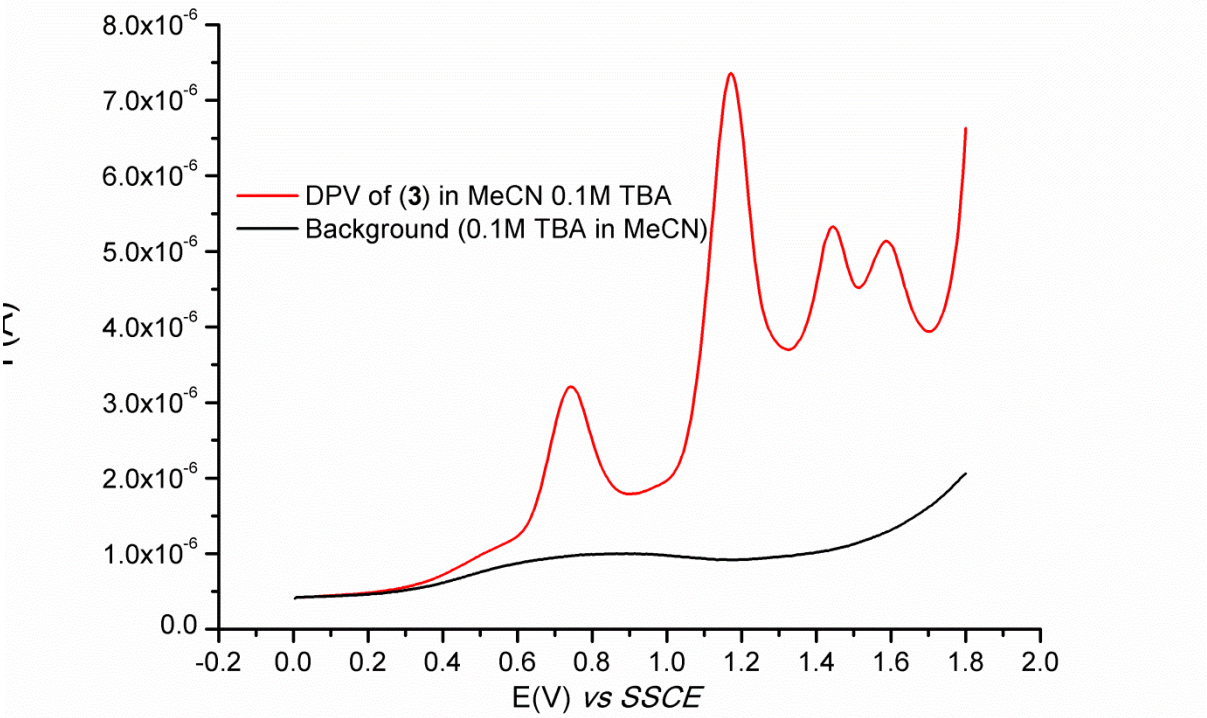

Figure S24. Differential pulse voltammetry diagram of catalyst **3** in MeCN 0.1 M TBA (tetrabutylammonium hexafluorophosphate) with a glassy carbon electrode.

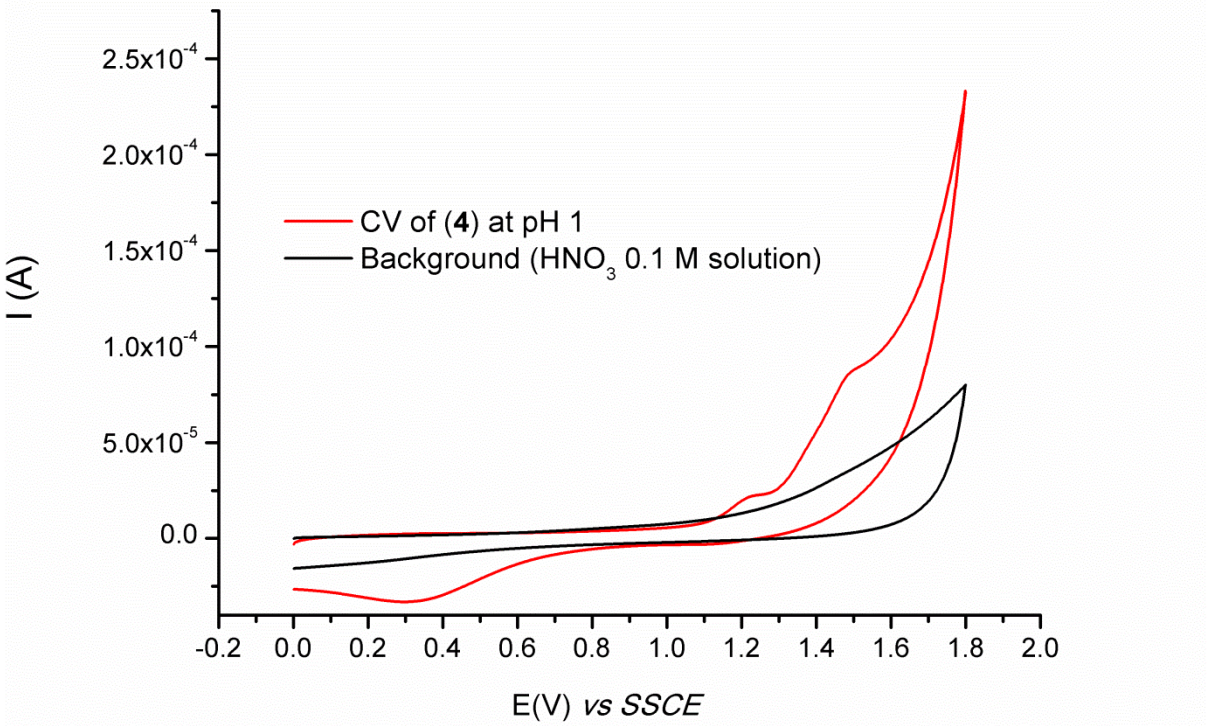

Figure S25. Cyclic voltammetry diagram (scan rate: 100mV/s) of catalyst **4** in HNO_3 0.1 M with a glassy carbon electrode.

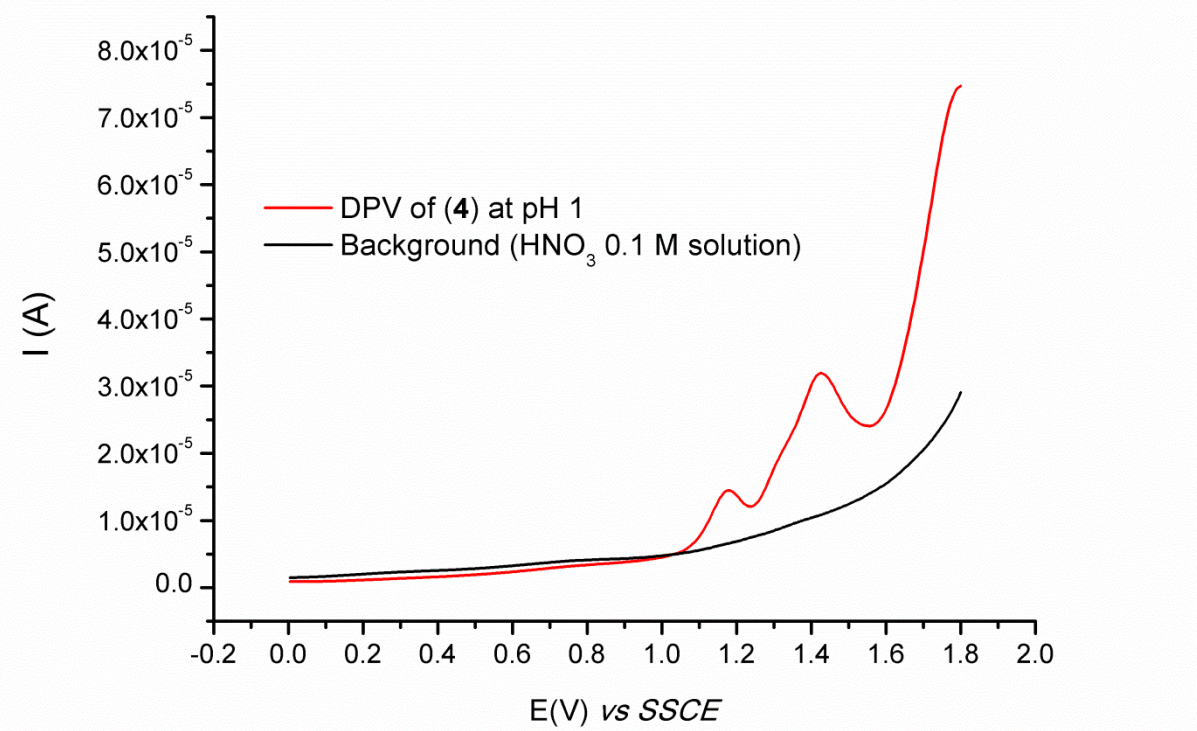

Figure S26. Differential pulse voltammetry diagram of catalyst **4** in HNO_3 0.1 M with a glassy carbon electrode.

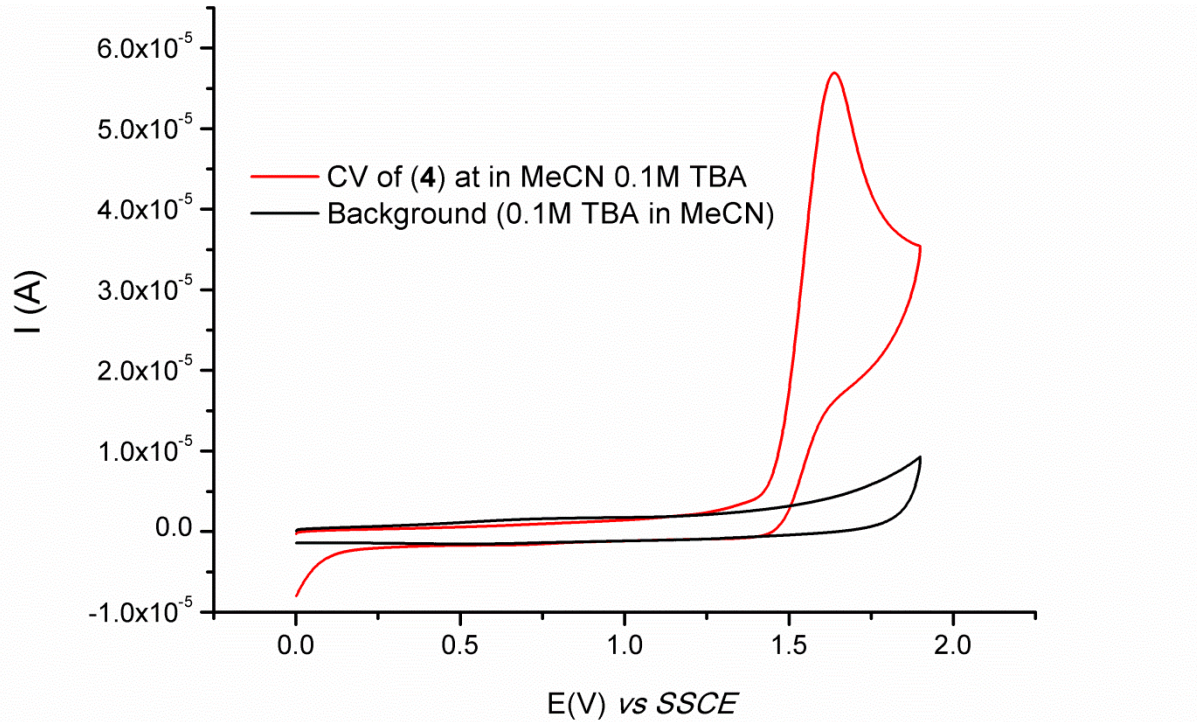

Figure S27. Cyclic voltammetry diagram (scan rate: 100mV/s) of catalyst **4** in MeCN 0.1 M TBA (tetrabutylammonium hexafluorophosphate) with a glassy carbon electrode.

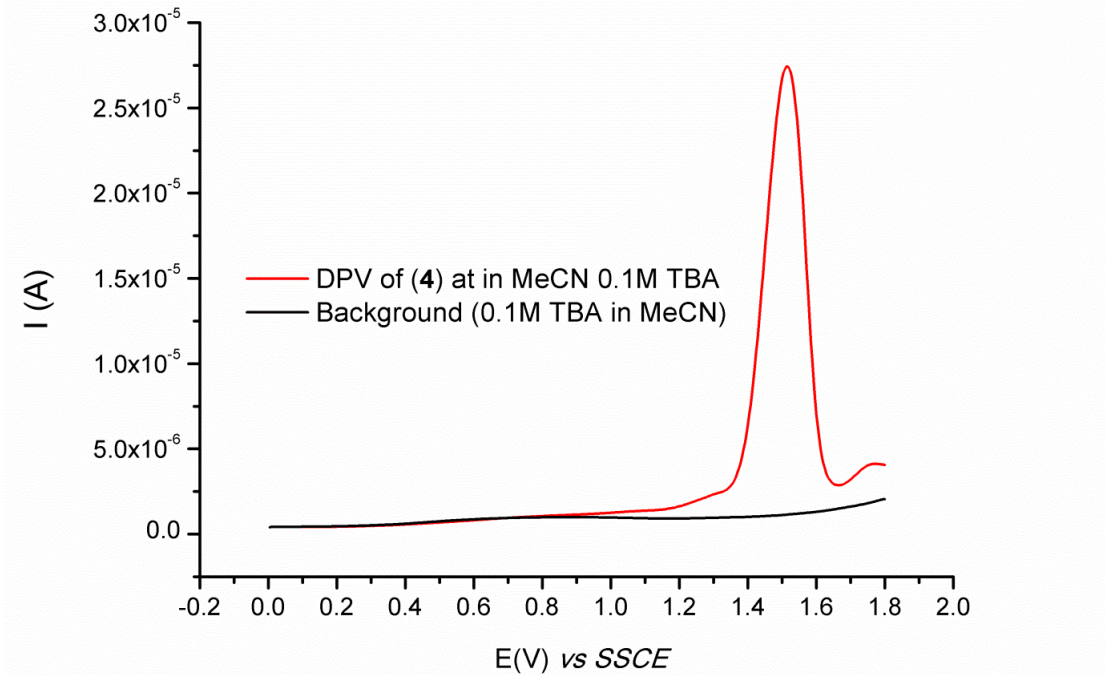

Figure S28. Differential pulse voltammetry diagram of catalyst **4** in MeCN 0.1 M TBA (tetrabutylammonium hexafluorophosphate) with a glassy carbon electrode.

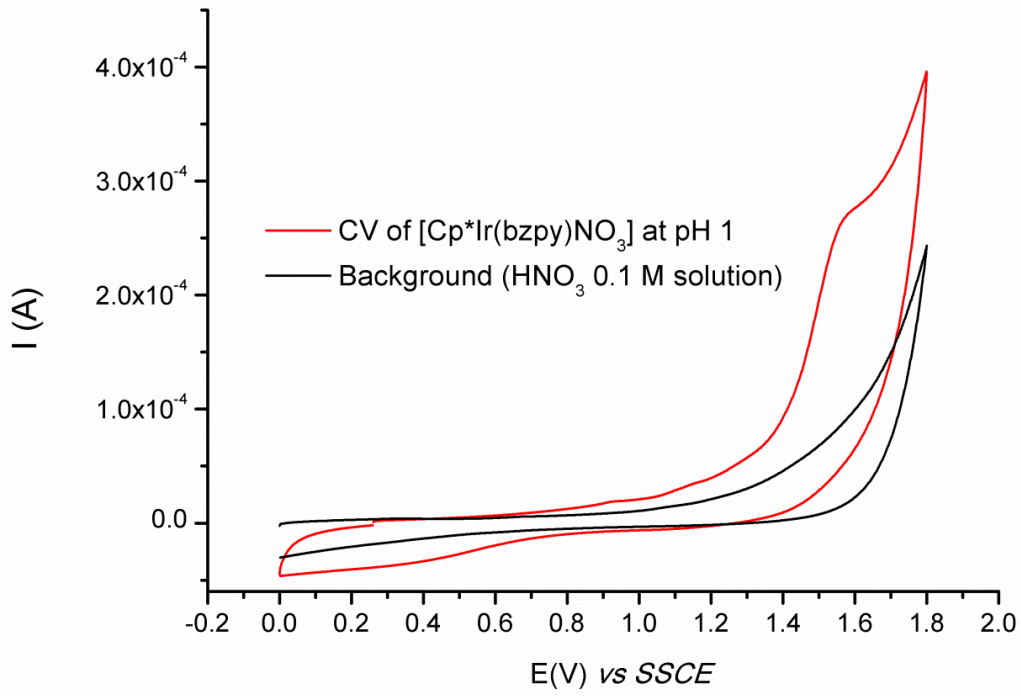

Figure S29. Cyclic voltammetry diagram (scan rate: 200 mV/s) of catalyst [$Cp^*Ir(bzpy)NO_3$] (bzpy = 2-benzoyl-pyridine) in HNO_3 0.1 M with a glassy carbon electrode.

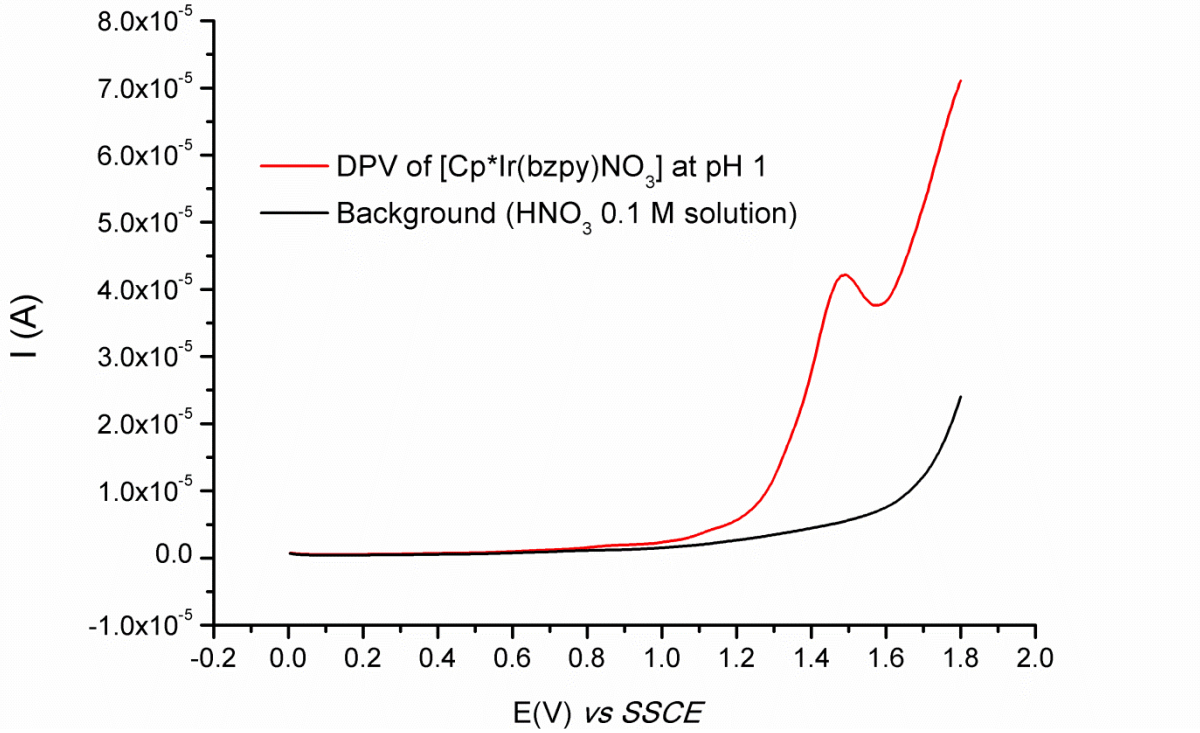

Figure S30. Differential pulse voltammetry diagram of catalyst [Cp*Ir(bzpy)NO_3] (bzpy = 2-benzoylpyridine) in HNO_3 0.1 M with a glassy carbon electrode.

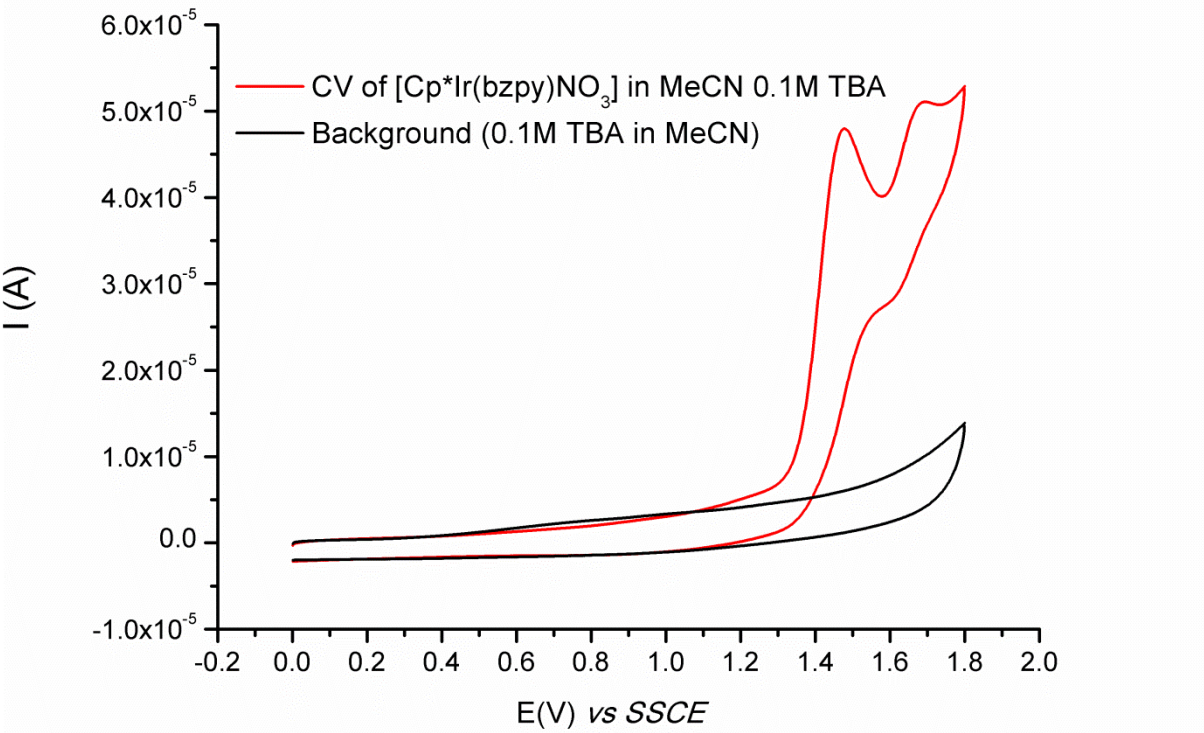

Figureure S31. Cyclic voltammetry diagram of catalyst [Cp*Ir(bzpy)NO_3] (bzpy = 2-benzoylpyridine) in MeCN 0.1 M TBA (tetrabutylammonium hexafluorophosphate) with a glassy carbon electrode.

Chemical water oxidation

Kinetic studies were conducted by: i) measuring the depletion of Ce^{+4} through a UV-Vis spectrophotometer, ii) directly detecting the evolved oxygen through the Clark electrode and iii) measuring the volume of the evolved oxygen.

i) UV-Vis experiments. Measurements of Ce^{+4} consumption were performed with a diode-array spectrometer (HP 8453). Two kind of experiments were carried out, the first one for the determination of long term TOF (TOF_{LT}) and the second one for the evaluation of TON. For the determination of TOF_{LT}, 200-2000 equivalents of CAN were added to the catalyst solution. In a typical catalytic run 1.5 mL of catalyst solution in 0.1 M HNO_3 (1.0–10.0 μM) was thermostated at 25°C into the cuvette for 20 min. After background correction, a solution of CAN in 0.1 M HNO_3 (1.5 mL, 2.0 mM) was added to the catalyst solution and the consumption of Ce^{+4} was monitored at 340 nm every 5 s. For the evaluation of TON a larger amount of CAN (4000-8000 eq.) was used. In a typical catalytic run 3.0 mL of 0.1 M HNO_3 solution was used for the background correction, then the acid solution was removed from the cuvette and 3 mL of a solution of CAN in 0.1 M HNO_3 (10.1 mM) was thermostated at 25°C for 20 min. Finally 30-40 μL of a catalyst solution (95-252 μM) were added into the cuvette. and the consumption of Ce^{+4} was monitored at 410 nm every 5 s.

ii) Evolved oxygen by Clark electrode. Measurements of initial oxygen evolution rate (TOF_{IN}) were performed with a Clark-type oxygen electrode (Hanna, model HI 4421). Before beginning each set of experiments, the gas-permeable membrane was replaced to ensure a high-quality response. The electrode, secured in a Teflon tube, was inserted into a tight-fitting water- jacketed glass vessel. The system was kept at a constant temperature of 25°C. In a typical experiment a CAN solution in 0.1M HNO_3 (25 mL, 2-77.4 mM) was allowed to equilibrate with stirring for 20 min. When a steady baseline was achieved, 0.6-0.8 mL of catalyst solution was added using a syringe through a septum. The catalyst concentration in

the total volume of reaction was 0.1-10.0 μM. Oxygen evolution commenced after an induction period and typically exceeded the maximum value for the system within 15 min of injection**.**

iii) Evolved oxygen by volumetry. Measurements of the turnover number (TON) of oxygen evolution were also performed with a custom-built apparatus. It consists of tight-fitting water-jacketed glass vessel equipped with a septum for the injection of the catalyst solution and with a side arm connected to a graduated Mohr bottle. The evolved O_2 was collected in the graduated Mohr bottle and all changes in volume were recorded by reading the numbers on it. Temperature and pressure were exactly measured in each experiment and they were used for the calculation of the amount of evolved oxygen. The flask was charged with a solution of CAN in 0.1 M HNO_3 (25 mL, 20.5–41.3 mM). The system was allowed to equilibrate at 25°C with stirring for 20 min. Finally a volume between 0.6 – 0.8 mL of the catalyst solution (161–213 μM) in 0.1 M HNO_3 was injected through the rubber septum. The CAN and the catalyst concentration in the total volume of reaction were, respectively, 20-40 mM and 5.0 μM.

Table S4. UV-Vis spectrophotometric results for [$Cp^*Ir(\kappa^2$-N,O)Cl] (**1a**).

C_{cat} (μM)	k_{obs} (Ms^{-1})[c]	TOF_{LT} (min^{-1})[d]	TON
1.00[a]	$(6.21 \pm 0.03)\cdot10^{-8}$	3.72 ± 0.03	250
1.00[a]	$(8.31 \pm 0.05)\cdot10^{-8}$	4.99 ± 0.02	250
2.00[a]	$(1.66 \pm 0.01)\cdot10^{-7}$	4.98 ± 0.03	125
2.00[a]	$(1.87 \pm 0.01)\cdot10^{-7}$	5.61 ± 0.03	125
3.00[a]	$(1.76 \pm 0.09)\cdot10^{-7}$	3.51 ± 0.02	83
3.00[a]	$(2.58 \pm 0.02)\cdot10^{-7}$	5.15 ± 0.03	83
4.00[a]	$(3.49 \pm 0.03)\cdot10^{-7}$	5.23 ± 0.04	62
4.00[a]	$(3.29 \pm 0.02)\cdot10^{-7}$	4.93 ± 0.03	62
5.00[a]	$(4.75 \pm 0.01)\cdot10^{-7}$	5.69 ± 0.02	50
5.00[a]	$(3.31 \pm 0.03)\cdot10^{-7}$	9.97 ± 0.03	50
1.25[b]	n/a	n/a	600
2.50[b]	n/a	n/a	1200

[a]$[Ce^{+4}]_0$ = 1.0 mM. [b]$[Ce^{+4}]_0$ = 10.0 mM. [c]From $(A_t/A_0)_{340nm}$ *versus* -4t/$[Ce^{+4}]_0$ trends. [d]From the k_{obs}/C_{cat} ratio.

In the experiments carried out with $[Ce^{+4}]_0$ = 1.0 mM, from k_{obs} *versus* C_{cat} trend, a mean value of TOF_{LT} = 0.082 s^{-1} (4.9 min^{-1}) was obtained. A $\log(k_{obs}) - \log(C_{cat})$ plot gave the order of reaction in catalyst. The slope of this straight line is 1.0 ± 0.1. A TON of 1200 was estimated by the experiments carried out with $[Ce^{+4}]_0$ = 10.0 mM

Table S5. Clark electrode results for [$Cp^*Ir(\kappa^2$-N,O)Cl] (**1a**).

C_{cat} (μM)	TOF_{IN} (min^{-1})[a]
0.10	120 ± 1
0.10	77 ± 1
0.50	120 ± 1
0.50	191.5 ± 0.8
0.50	287 ± 3
1.00	244 ± 3
1.00	195 ± 2
2.50	143 ± 2
2.50	128 ± 2
5.00	74 ± 2
5.00	42.6 ± 0.3
5.00	41.8 ± 0.4
5.00	84 ± 1
10.0	71 ± 1
10.0	70 ± 1

[a]From the $[O_2]$ *versus* t ($[Ce^{+4}]_0$=20.0 mM), divided by C_{cat}.

The average value for TOF_{IN} is 126 ± 73 min^{-1} (± standard deviation).

Table S6. UV-Vis spectrophotometric results for $[Cp^*Ir(\kappa^2\text{-}N,O)NO_3]$ (**1b**).

C_{cat} (μM)	k_{obs} (Ms^{-1})[c]	TOF_{LT} (min^{-1})[d]	TON
0.50[a]	$(1.80 \pm 0.01)\cdot10^{-8}$	2.10 ± 0.04	500
0.50[a]	$(2.50 \pm 0.01)\cdot10^{-8}$	3.00 ± 0.04	500
1.00[a]	$(8.20 \pm 0.02)\cdot10^{-8}$	4.9 ± 0.03	250
1.00[a]	$(9.20 \pm 0.01)\cdot10^{-8}$	5.5 ± 0.03	250
2.00[a]	$(1.92 \pm 0.01)\cdot10^{-7}$	5.8 ± 0.02	125
2.00[a]	$(1.87 \pm 0.01)\cdot10^{-7}$	5.6 ± 0.03	125
3.00[a]	$(2.48 \pm 0.01)\cdot10^{-7}$	5.0 ± 0.02	83
3.00[a]	$(3.00 \pm 0.03)\cdot10^{-7}$	6.0 ± 0.01	83
4.00[a]	$(2.77 \pm 0.03)\cdot10^{-7}$	4.2 ± 0.02	62
4.00[a]	$(3.70 \pm 0.03)\cdot10^{-7}$	5.6 ± 0.05	62
5.00[a]	$(4.20 \pm 0.01)\cdot10^{-7}$	5.0 ± 0.01	50
5.00[a]	$(2.40 \pm 0.01)\cdot10^{-7}$	2.9 ± 0.01	50
1.25[b]	n/a	n/a	2000
2.5[b]	n/a	n/a	1000

[a]$[Ce^{+4}]_0$ = 1.0 mM. [b]$[Ce^{+4}]_0$ = 10.0 mM. [c]From $(A_t/A_0)_{340nm}$ *versus* -4t/$[Ce^{+4}]_0$ trends. [d]From the k_{obs}/C_{cat} ratio.

In the experiments carried out with $[Ce^{+4}]_0$ = 1.0 mM, from k_{obs} *versus* C_{cat} trend, a mean value of TOF_{LT} = 0.071 s^{-1} (4.3 min^{-1}) was obtained. A $\log(k_{obs}) - \log(C_{cat})$ plot gave the order of reaction in catalyst. The slope of this straight line is 1.2 ± 0.1. A TON value of 2000 was estimated by the experiments carried out with $[Ce^{+4}]_0$ = 10.0 mM.

Table 7S. Clark electrode results for [$Cp^*Ir(\kappa^2$-N,O)NO_3] (**1b**).

C_{cat} (μM)	C_{CAN} (mM)	TOF_{IN} (min^{-1})[a]
0.50	40.0	222 ± 5
0.50	40.0	251 ± 4
1.00	40.0	277 ± 6
1.00	20.0	69.3 ± 0.5
1.00	20.0	97 ± 2
1.00	20.0	52.2 ± 0.6
1.00	20.0	60.6 ± 0.6
1.00	20.0	42 ± 1
1.00	20.0	84 ± 1
1.00	20.0	70.4 ± 0.4
3.75	20.0	107 ± 2
5.00	40.0	105 ± 1
5.00	40.0	69 ± 1
5.00	20.0	117 ± 3
5.00	20.0	44.4 ± 0.4
5.00	20.0	103 ± 2

[a]From the [O_2] *versus* t, divided by C_{cat}.

The average value for TOF_{IN} is 111 ± 70 min^{-1} (± standard deviation).

Table 11S. UV-Vis spectrophotometric results for [$Cp^*Ir(\kappa^2$-N,O)Cl] (**2**).

C_{cat} (μM)	k_{obs} (Ms^{-1})[c]	TOF_{LT} (min^{-1})[d]	TON
0.50[a]	$(2.50 \pm 0.05)\cdot10^{-8}$	2.9947 ± 0.0001	500
0.50[a]	$(2.98 \pm 0.05)\cdot10^{-8}$	3.5803 ± 0.0001	500
1.00[a]	$(5.73 \pm 0.01)\cdot10^{-8}$	3.4447 ± 0.0001	250
1.00[a]	$(5.68 \pm 0.08)\cdot10^{-8}$	3.4121 ± 0.0001	250
2.00[a]	$(1.15 \pm 0.01)\cdot10^{-7}$	3.4480 ± 0.0001	125
2.00[a]	$(1.03 \pm 0.01)\cdot10^{-7}$	3.0966 ± 0.0001	125
3.00[a]	$(1.57 \pm 0.03)\cdot10^{-7}$	3.1354 ± 0.0001	83
3.00[a]	$(1.48 \pm 0.01)\cdot10^{-7}$	2.9552 ± 0.0004	83
4.00[a]	$(1.95 \pm 0.01)\cdot10^{-7}$	2.9185 ± 0.0001	62
4.00[a]	$(2.08 \pm 0.03)\cdot10^{-7}$	3.1374 ± 0.0001	62
5.00[a]	$(2.18 \pm 0.05)\cdot10^{-7}$	2.6323 ± 0.0001	50
5.00[a]	$(2.08 \pm 0.05)\cdot10^{-7}$	2.4942 ± 0.0001	50
1.25[b]	n/a	n/a	750
2.50[b]	n/a	n/a	400

[a]$[Ce^{+4}]_0$ = 1.0 mM. [b]$[Ce^{+4}]_0$ = 10.0 mM. [c]From $(A_t/A_0)_{340nm}$ *versus* -4t/$[Ce^{+4}]_0$ trends. [d]From the k_{obs}/C_{cat} ratio.

In the experiments carried out with $[Ce^{+4}]_0$ = 1.0 mM, from k_{obs} *versus* C_{cat} trend, a mean value of TOF_{LT} = 0.043 s^{-1} (2.6 min^{-1}) was obtained. A $\log(k_{obs}) - \log(C_{cat})$ plot gave the order of reaction in catalyst. The slope of this straight line is 0.91 ± 0.03. A TON value of 750 was estimated by the experiments carried out with $[Ce^{+4}]_0$ = 10.0 mM.

Table 12S. Clark electrode results for [$Cp^*Ir(\kappa^2$-N,O)Cl] (**2**).

C_{cat} (μM)	C_{CAN} (mM)	TOF_{IN} (min^{-1})[a]
1.00	20.0	43.4 ± 0.6
1.00	20.0	36.4 ± 0.3
1.00	20.0	29.8 ± 0.2
1.00	40.0	30.9 ± 0.4
1.00	40.0	30.2 ± 0.6
5.00	20.0	12.2 ± 0.2
5.00	20.0	9.66 ± 0.09
5.00	20.0	10.05 ± 0.08
5.00	40.0	15.4 ± 0.1
5.00	40.0	17.4 ± 0.2

[a]From the [O_2] *versus* t, divided by C_{cat}.

The average value for TOF_{IN} is 23 ± 12 min^{-1} (± standard deviation).

Table 8S. UV-Vis spectrophotometric results for [$Cp^*Ir(\kappa^2$-N,O)Cl] (**3**).

C_{cat} (μM)	k_{obs} (Ms^{-1})[a]	TOF_{LT} (min^{-1})[b]	TON
0.50	$(4.38 \pm 0.04)\cdot10^{-8}$	5.260 ± 0.005	500
0.50	$(4.04 \pm 0.05)\cdot10^{-8}$	4.853 ± 0.006	500
1.00	$(7.78 \pm 0.02)\cdot10^{-8}$	4.67 ± 0.01	250
1.00	$(1.06 \pm 0.05)\cdot10^{-7}$	6.39 ± 0.03	250
1.50	$(1.28 \pm 0.04)\cdot10^{-7}$	5.12 ± 0.01	167
2.00	$(1.78 \pm 0.05)\cdot10^{-7}$	5.34 ± 0.01	125
2.00	$(1.63 \pm 0.01)\cdot10^{-7}$	4.902 ± 0.003	125
2.50	$(2.79 \pm 0.04)\cdot10^{-7}$	6.68 ± 0.01	100
3.00	$(2.95 \pm 0.08)\cdot10^{-7}$	5.90 ± 0.02	83
3.00	$(3.18 \pm 0.06)\cdot10^{-7}$	6.35 ± 0.01	83
3.50	$(3.18 \pm 0.08)\cdot10^{-7}$	5.45 ± 0.01	71
4.00	$(3.67 \pm 0.01)\cdot10^{-7}$	5.51 ± 0.01	62
4.00	$(4.49 \pm 0.02)\cdot10^{-7}$	6.74 ± 0.03	62
4.50	$(5.60 \pm 0.02)\cdot10^{-7}$	7.46 ± 0.03	56
5.00	$(5.83 \pm 0.04)\cdot10^{-7}$	7.00 ± 0.01	50
5.00	$(5.24 \pm 0.03)\cdot10^{-7}$	6.29 ± 0.04	50

[a]From $(A_t/A_0)_{340nm}$ *versus* $-4t/[Ce^{+4}]_0$ trends ($[Ce^{+4}]_0$ = 1.0 mM). [b]From the k_{obs}/C_{cat} ratio.

From k_{obs} *versus* C_{cat} trend, a mean value of TOF_{LT} = 0.116 s^{-1} (7.0 min^{-1}) was obtained. A $\log(k_{obs}) - \log(C_{cat})$ plot gave the order of reaction in catalyst. The slope of this straight line is 1.12 ± 0.04.

Table 9S. Clark electrode results for [$Cp^*Ir(\kappa^2$-N,O)Cl] (**3**).

C_{cat} (μM)	C_{CAN} (mM)	TOF_{IN} (min^{-1})[a]
1.00	10.0	29.6 ± 0.3
1.00	20.0	14.4 ± 0.1
5.00	2.0	5.74 ± 0.04
5.00	20.0	19.8 ± 0.4
5.00	75.0	14.6 ± 0.3

[a]From the $[O_2]$ *versus* t, divided by C_{cat}.

The average value for TOF_{IN} is 17 ± 9 min^{-1} (± standard deviation).

Table 10S. Volumetric results for [$Cp^*Ir(\kappa^2$-N,O)Cl] (**3**).

C_{cat} (μM)	C_{CAN} (mM)	TOF_{LT} (min^{-1})[a]	TON
5.00	20.0	4.7 ± 0.1	1000
5.00	40.0	8.4 ± 0.2	1300

[a]From the mol of evolved gas *versus* t, divided by mol_{cat}.

Table 13S. UV-Vis results for [Ir(κ^3-N,O,O)(1-κ-4,5-η^2-C_8H_{13})(MeOH)] (**4**)

C_{cat} (μM)	k_{obs} (Ms^{-1})[c]	TOF_{LT} (min^{-1})[d]	TON
0.50[a]	$(4.88 \pm 0.04)\cdot10^{-8}$	5.856 ± 0.005	500
0.50[a]	$(4.54 \pm 0.08)\cdot10^{-8}$	5.45 ± 0.01	500
0.50[a]	$(4.97 \pm 0.01)\cdot10^{-8}$	5.964 ± 0.003	500
1.00[a]	$(1.11 \pm 0.02)\cdot10^{-7}$	6.667 ± 0.006	250
1.00[a]	$(1.24 \pm 0.05)\cdot10^{-7}$	7.44 ± 0.01	250
2.00[a]	$(2.74 \pm 0.04)\cdot10^{-7}$	8.22 ± 0.01	125
2.00[a]	$(2.77 \pm 0.06)\cdot10^{-7}$	8.31 ± 0.01	125
3.00[a]	$(4.00 \pm 0.01)\cdot10^{-7}$	8.00 ± 0.01	83
3.00[a]	$(4.04 \pm 0.02)\cdot10^{-7}$	8.08 ± 0.02	83
4.00[a]	$(5.38 \pm 0.01)\cdot10^{-7}$	8.07 ± 0.03	62
4.00[a]	$(5.23 \pm 0.03)\cdot10^{-7}$	7.84 ± 0.01	62
5.00[a]	$(5.72 \pm 0.02)\cdot10^{-7}$	6.86 ± 0.04	50
5.00[a]	$(5.65 \pm 0.01)\cdot10^{-7}$	6.78 ± 0.02	50
2.50[b]	n/a	n/a	500

[a]$[Ce^{+4}]_0$ = 1.0 mM. [b]$[Ce^{+4}]_0$ = 10.0 mM. [c]From $(A_t/A_0)_{340nm}$ *versus* -4t/$[Ce^{+4}]_0$ trends. [d]From the k_{obs}/C_{cat} ratio.

In the experiments carried out with $[Ce^{+4}]_0$ = 1.0 mM, from k_{obs} *versus* C_{cat} trend, a mean value of TOF_{LT} = 0.123 s^{-1} (7.4 min^{-1}) was obtained. A $\log(k_{obs}) - \log(C_{cat})$ plot gave the order of reaction in catalyst. The slope of this straight line is 1.11 ± 0.03. A TON value of 500 was estimated by the experiment carried out with $[Ce^{+4}]_0$ = 10.0 mM.

Table 14S. Clark electrode results for [Ir(κ^3-N,O,O)(1-κ-4,5-η^2-C_8H_{13})(MeOH)] (**4**)

C_{cat} (μM)	TOF_{IN} (min^{-1})[a]
1.00	5.2 ± 0.1
1.00	6.8 ± 0.09
2.50	3.42 ± 0.05
2.50	4.02 ± 0.03
5.00	5.1 ± 0.1
5.00	7.60 ± 0.09
5.00	5.90 ± 0.07

[a]From the $[O_2]$ *versus* t, divided by C_{cat} ($[Ce^{+4}]_0$ = 20.0 mM).

The average value for TOF_{IN} is 5 ± 1 min^{-1} (± standard deviation).

References

1. Ziessel, R. *J. Chem. Soc., Chem. Commun.* **1988**, 16–17.
2. Poth, T.; Paulus, H.; Elias, H.; Dücker-Benfer, C.; van Eldik, R. *Eur. J. Inorg. Chem.* **2001**, *2001*, 1361-1369. Gorol, M.; Roesky, H. W.; Noltemeyer, M.; Schmidt, H.-G. *Eur. J. Inorg. Chem.* **2005**, 4840-4844.
3. Nguyen, D. H.; Perez-Torrente, J. J.; Lomba, L.; Jimenez, M. V.; Lahoza, F. J.; Oro, L. A. *Dalton Trans.* **2011**, *40*, 8429–8435.
4. *BrukerAXS, SAINT*; Bruker Analytical X-ray Systems, Madison, WI, 1995.
5. Sheldrick, G. M. *SADABS*, Program for Absorption Correction; University of Göttingen, Göttingen, Germany, 1996.
6. Sheldrick, G. M. *Acta Crystallogr.*. **2008**, *A64*, 112.
7. Flack, H. D. *Acta Crystallogr.* **1983**, *A39*, 876
8. Farrugia, L .J. *J. Appl. Crystallogr.* **1997**, *30*, 565; *J. Appl. Crystallogr.* **1999**, *32*, 837.
9. *Mercury* CSD 3.0.1 (Build RC6), The Cambridge Crystallographic Data Center, Cambridge, UK, 2011